RESEARCH ARTICLE

Long-term persistence of infectious Zika virus: Inflammation and behavioral sequela in mice

Derek D. C. Ireland[1], **Mohanraj Manangeeswaran**[1], **Aaron P. Lewkowicz**[1], **Kaliroi Engel**[1], **Sarah M. Clark**[2], **Adelle Laniyan**[2], **Jacob Sykes**[1], **Ha-Na Lee**[1], **Ian L. McWilliams**[1], **Logan Kelley-Baker**[1], **Leonardo H. Tonelli**[2], **Daniela Verthelyi**[1] *

1 US Food and Drug Administration, Office of Biotechnology Products, Silver Spring, Maryland, United States of America, **2** University of Maryland School of Medicine, Department of Psychiatry, Baltimore, Maryland, United States of America

* daniela.verthelyi@fda.hhs.gov

Abstract

The neurodevelopmental defects associated with ZIKV infections early in pregnancy are well documented, however the potential defects and long-term consequences associated with milder infections in late pregnancy and perinatal period are less well understood. To model these, we challenged 1 day old (P1) immunocompetent C57BL/6 mice with ZIKV. The animals developed a transient neurological syndrome including unsteady gait, kinetic tremors, severe ataxia and seizures 10–15 days post-infection (dpi) but symptoms subsided after a week, and most animals survived. Despite apparent recovery, MRI of convalescent mice show reduced cerebellar volume that correlates with altered coordination and motor function as well as hyperactivity and impulsivity. Persistent mRNA levels of pro-inflammatory genes including *Cd80*, *Il-1α*, and *Ifn-γ* together with *Cd3*, *Cd8* and perforin (*PrfA*), suggested persistence of low-grade inflammation. Surprisingly, the brain parenchyma of convalescent mice harbor multiple small discrete foci with viral antigen, active apoptotic processes in neurons, and cellular infiltrates, surrounded by activated astrocytes and microglia as late as 1-year post-infection. Detection of negative-sense strand viral RNA and isolation of infectious virus derived from these convalescent mice by blinded passage in Vero cells confirmed long-term persistence of replicating ZIKV in CNS of convalescent mice. Although the infection appears to persist in defined reservoirs within CNS, the resulting inflammation could increase the risk of neurodegenerative disorders. This raises concern regarding possible long-term effects in asymptomatic children exposed to the virus and suggests that long-term neurological and behavioral monitoring as well as anti-viral treatment to clear virus from the CNS may be useful in patients exposed to ZIKV at an early age.

Author summary

Infections in the perinatal period are associated with lasting cognitive impairment and increased risk for affective disorders. The congenital brain malformations associated with ZIKV infections early in pregnancy are well documented, however whether perinatal exposure could lead to long term sequelae is not fully understood. Using a non-lethal

neonatal mouse model of ZIKV, we examine host-pathogen interactions, anatomical changes and behavioral patterns by following survivors of the acute infection for over 1 year. We discover that ZIKV has the potential to remain in the CNS for extended periods, lodged within small foci surrounded by gliosis and infiltrating immune cells that may act to limit the viral spread, but also interfere with healing and contribute to ongoing neuropathic and behavioral sequelae. This suggests anti-viral treatment and long-term neurological and behavioral monitoring may be indicated for patients exposed to ZIKV early in life.

Introduction

Zika virus (ZIKV) is an arbovirus from the Flaviviridae family that caused a world-wide public health emergency between 2014 and 2016 as over 750,000 cases were reported in 84 countries, including over 40,000 in the US [1]. Although transmission of ZIKV has since declined, WHO now considers Zika endemic to many areas of the world and infection clusters continue to be reported in regions of Cuba, India and Southeast Asia, where there are large populations of women of childbearing age who are susceptible to the virus [2–5]. Zika infections are asymptomatic in most adults, but approximately 20% of patients develop fever, rash, conjunctivitis, muscle and joint pain [6]. In a small number of cases ZIKV infections have been linked to more serious neurological disease including: Guillain Barre Syndrome, acute myelitis, encephalitis and polyneuropathies, as well as chorioretinitis [7,8]. Importantly, infections are more detrimental during early pregnancy as ~10% of children born to mothers infected during the 1st trimester show developmental defects at birth including microencephaly, lissencephaly, cerebral atrophy, ventriculomegaly, cerebellar hypoplasia, brain calcifications, microphthalmia, and arthrogryposis [9–12]. These defects have been collectively termed congenital Zika syndrome. Among the children of women exposed during the second and third trimester, the incidence of Zika congenital syndrome was lower, but there are multiple reports of neurodevelopmental defects, hydrocephaly, seizures, hearing, motor, behavioral and sociability deficits, suggesting that Zika's pathological effect extends beyond the early developmental period [13]. Importantly these defects can be evident at birth or develop later in life suggesting that the full neurological and behavioral impact of this disease may become apparent as these children grow [13,14]. Further, reports of virus in the spinal fluid months after birth suggest a delay in full viral clearance from the CNS [15]. Thus, it is critical to gain a better understanding of the host-pathogen interactions, both during acute infection and after apparent recovery, to identify possible interventions to reduce the developmental impact and minimize the damage that viral persistence could cause.

To better understand the long-term effects of ZIKV infections our group developed a model using immunocompetent C57BL/6 mice (B6) challenged at one day after birth (P1) with ZIKV (PRVABC059 strain, subcutaneous route) [16]. Previous studies comparing human and mouse CNS developmental markers such as stages of neurogenesis, axon extension, establishment and refinement of synapses, and myelin formation, indicated that a the brain developmental stage of a mouse at P1 roughly corresponds to the second to third trimester pregnancy of a human brain [17,18]. We have previously shown that C57BL/6 mice infected at P1 with ZIKV develop a transient encephalitis characterized by unsteady gait, kinetic tremors, severe ataxia, loss of balance and seizures that manifest 10–12 days post infection (dpi) and subside by 26–30 dpi [16]. CNS infection leads to inflammation, cellular infiltration predominantly of CD8+ T cells, and increased mRNA expression levels of interferon-gamma (*Ifn-γ*),

granzyme B (*GzmB*), and perforin (Prf1), that are associated with neurodegeneration and loss of Purkinje cells [16]. Over 80% of the mice survive the challenge and live a normal life span, without displaying ataxia, seizure or other overt signs of neurological deficit. The non-lethal outcome allows for the study of the natural progression of ZIKV infection in a developing brain and any resulting structural and functional deficits. Importantly, by challenging mice at P1, rather than challenging pregnant dams, this mouse model bypasses the maternal immune response and placental insufficiency, which are known to impact on neurological development and can confound the effects of the infection.

Recent studies assessing the effects of Zika infections showed that mice can have behavioral and motor deficits as late as 60 dpi [19] and the chorioretinitis that affects these mice is evident as late as 90 dpi [20]. In this study, we follow the natural history of the surviving mice and show that although the signs of acute encephalitis subside, the mice have significant long-term deficits in motor function, coordination and anxiety that correlate with reduced brain volume, particularly affecting the cerebellum. We further show that, replicating Zika virus persists in the brain of surviving mice within foci that are surrounded by activated astrocytes and microglia for more than 1 year, and is associated with ongoing apoptosis. The relative contribution of the original tissue damage and the persistent ZIKV replication and surrounding inflammation in the CNS, to the observed neurological deficits in adults remains unclear, however it suggests that the virus and the immune system in the CNS reach an equilibrium that allows the virus to survive without egressing from the CNS to seed peripheral organs. These studies raise the possibility that individuals exposed to Zika early in development may not only experience long-term sequelae associated with the tissue damage that occurs during acute infection, but also have continuous foci of persistent inflammation in their CNS parenchyma that limit the spread of live replicating virus but may worsen their long-term prognosis.

Results

Acute Zika infection in CNS in neonatal mice

Subcutaneous infection with ZIKV in neonatal (P1) C57BL/6 mice leads to a transient viremia, followed by infection of the CNS (Fig 1A) [16,20]. As previously published, the virus is cleared from peripheral blood and most organs within 9 dpi, but in the CNS viral RNA peaks at 6–12 dpi and persists long after symptoms have resolved (Fig 1A) [16,21]. At 12 dpi, IF-IHC shows ZIKV antigen primarily in the cortex, hippocampus, and cerebellum (Fig 1B), however animals recover and by 30 dpi little residual viral antigen can be detected, even in tissues that had been heavily infected such as the cerebellum (Fig 1B). The clinical evolution of the encephalitis follows the viral load and the symptoms, which include reduced weight gain, ataxia, dystonia, and seizures, resolve by 24 dpi [16,22–24]. Overall, fewer than 20% of the animals succumb to infection and surviving animals live more than 2 years with higher than 80% surviving by 12 months. (Fig 1A).

During the acute infection there is significant meningitis and swelling of the pia as well as extensive cellular infiltration with increased numbers of CD45^{+} lymphocytes and Iba-1^{+} activated microglia evident in the infected areas, particularly in cerebellum, (Figs 1C and S1). Assessment of immune-related gene expression suggests that inflammation peaks at 15 dpi, as there is increased expression of genes linked to interferon responses (*Ifnα, Ifnβ, Irf7, Ifi204, Slamf7*); recruitment and activation of macrophages and neutrophils (*Ccl2, Ccl5, Cxcl10, Cxcl11, Cxcr2, Cxcr6*); antigen presentation (MHC (*H2-Aa, -Ab1, -Eb1, -K1*), *B2m, Cd74, Tap1, Psamb9, Cd274, Cd80, Cd86*), and inflammation (*C3, Tnf, Il1, Il18, Il6, and Casp1*), as well as genes that suggest the presence of infiltrating T and NK cells (*Cd3, Cd4 and Cd8, Il2, Gzma/b and Prf1, Klrc1, Kirk1, and Ifnγ*) (Fig 1D). The infected areas show significant TUNEL
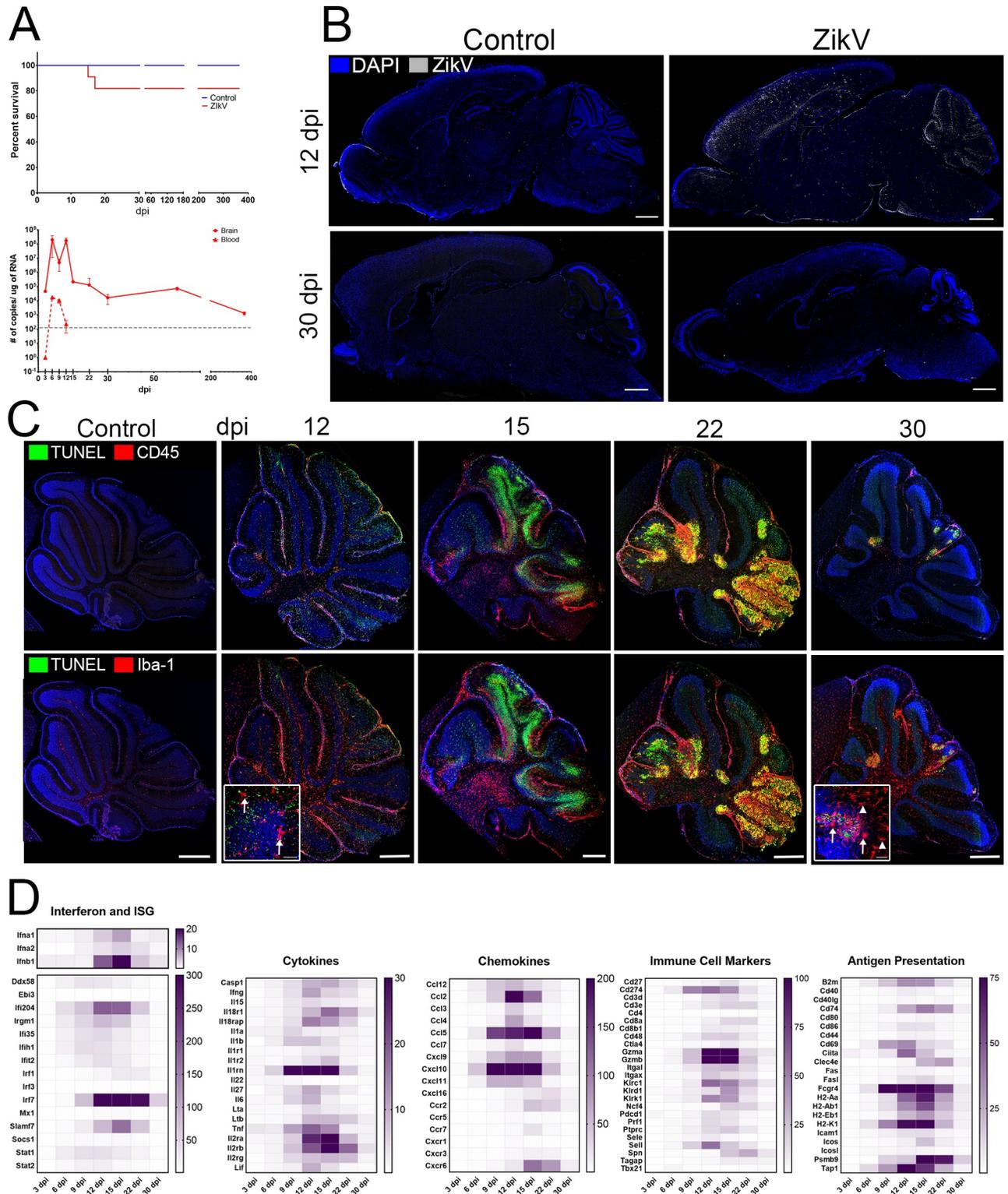
Fig 1. Acute ZIKV infection in CNS. Neonatal C57Bl/6 mice were challenged with 2000 TCID$_{50}$ SC on P1. **A.** Top. Survival curve. 20% of animals succumb to disease by 18 dpi, 80% survive (n > 20/group). Bottom. Viral RNA copies/μg RNA in CNS and blood. By 15 dpi (peak of symptomatic disease) ZIKV RNA levels are significantly reduced relative to peak viral RNA levels (9–12 dpi) (n = 6 mice/timepoint). After symptoms subside, viral RNA is persistently detectable in the CNS of the animal. **B.** Sagittal brain sections of ZIKV infected and aged-match controls stained for ZIKV. Image shows representative image of 4–6 animals per time point; scale bar = 1 mm. **C.** Cerebellum of ZIKV infected animals at indicated dpi. Top: Staining for

CD45+ infiltrating immune cells (red) and apoptosis (TUNEL, green). Bottom: Staining with TUNEL (green) and Iba-1+ microglia (red) indicating microgliosis. Both infiltrating immune cells and activated microglia progressively colocalize with distinct apoptotic foci in the cerebellum. Scale bar = 500 μm. Insets. Confocal maximum projection of TUNEL and Iba-1+ microglia in granular layer of cerebellum. Arrows indicate activated microglia. Arrow heads indicated resting microglia, distal from apoptotic foci at 30 dpi. Scale bar = 50 μm. **D.** Heatmap of RNA expression (fold change, n = > 6 infected, n = > 3 uninfected from at least 2 independent experiments per time point in the brain of ZIKV-infected animals, from 3 dpi to 30 dpi, as detected by Nanostring technology. Genes selected based on significant changes during disease course, from a panel of 596 genes and organized by gene function. A full table is available upon demand.

https://doi.org/10.1371/journal.ppat.1008689.g001

staining indicating extensive apoptosis and neurodegeneration in cerebellum that results in a disorganization of cerebellar cortex and reduced number of Purkinje cells (Figs 1C and S2A), although areas of apoptosis are also evident in the occipital cerebral cortex and hippocampus (S2B Fig). Importantly, as the viral load decreases and the symptoms subside, cellular infiltration and gliosis in cerebellum resolve, and inflammation of the pia diminishes (Figs 1C and S1). Together, these data suggested that ZIKV causes a symptomatic but transient meningoencephalitis in neonatal mice.

Increased levels of fluid in CNS and reduced cerebellum volume in convalescent mice

While ZIKV-infected mice older than 30 days showed no obvious tremors, ataxia or seizures, the extensive tissue disruption during acute disease suggested that the transient infection could result in enduring loss of cerebral mass or calcifications paralleling the lesions described for exposed human offspring. To evaluate whether the infection led to long-term structural damage, we performed magnetic resonance imaging (MRI) of infected mice at 60 dpi ("young"), 4–6 ("adult"), and 12–14 ("aged") months post-infection (mpi). As shown in Fig 2, at 60 dpi the overall volume of the brain was smaller compared to controls, consistent with recently published findings [19]. Of note, as the mice age and catch-up in body weight (S3 Fig), the differences in total brain volume relative to age-matched controls became less evident suggesting that the tissue repairs over time (Fig 2B). However, convalescent animals showed increased percentage fluid (as indicated by white) in the CNS, especially in and around cerebellum and a reduction in cerebellar volume that was evident at all the time points. This fluid increase appears to be associated with expansion of the 4th ventricle and/or the thickness of the pia layers surrounding the cerebellum but may also reflect changes to the microstructural composition of the tissue. Therefore, although animals that survived neonatal ZIKV infection with PRVABC059 do not exhibit overt microcephaly, they do have reduced cerebellar volume and increased cerebellar fluid. Importantly, multiple studies have shown that defects in cerebellum can affect not only balance and coordination, but language, emotion, social behavior and working memory as well [25,26].

Perinatal ZIKV infection results in long-term motor and behavior defects

Despite the reduction in cerebellar volume, the behavior of convalescent mice in their home cage environment was grossly indistinguishable from age-matched control mice. To examine more closely whether the early infection resulted in functional sequelae, we tested locomotor activity, as well as social, emotional and learning behavior of convalescent mice in three age groups: "young adult" (60 dpi), "adults" (4–6 months post infection (mpi)) and "aged" (> 1-year post infection (ypi)) mice. All animals were exposed to the same battery of 5 tests, under the same conditions and in the same environment, by a blinded researcher. The rotarod test, which examines motor function and coordination (Fig 3A) showed a significant reduction in latency to fall among ZIKV-infected mice for all ages compared to age-matched controls, revealing an impairment in motor coordination and endurance (U = 253; *p < 0.0001;* Fig 3).
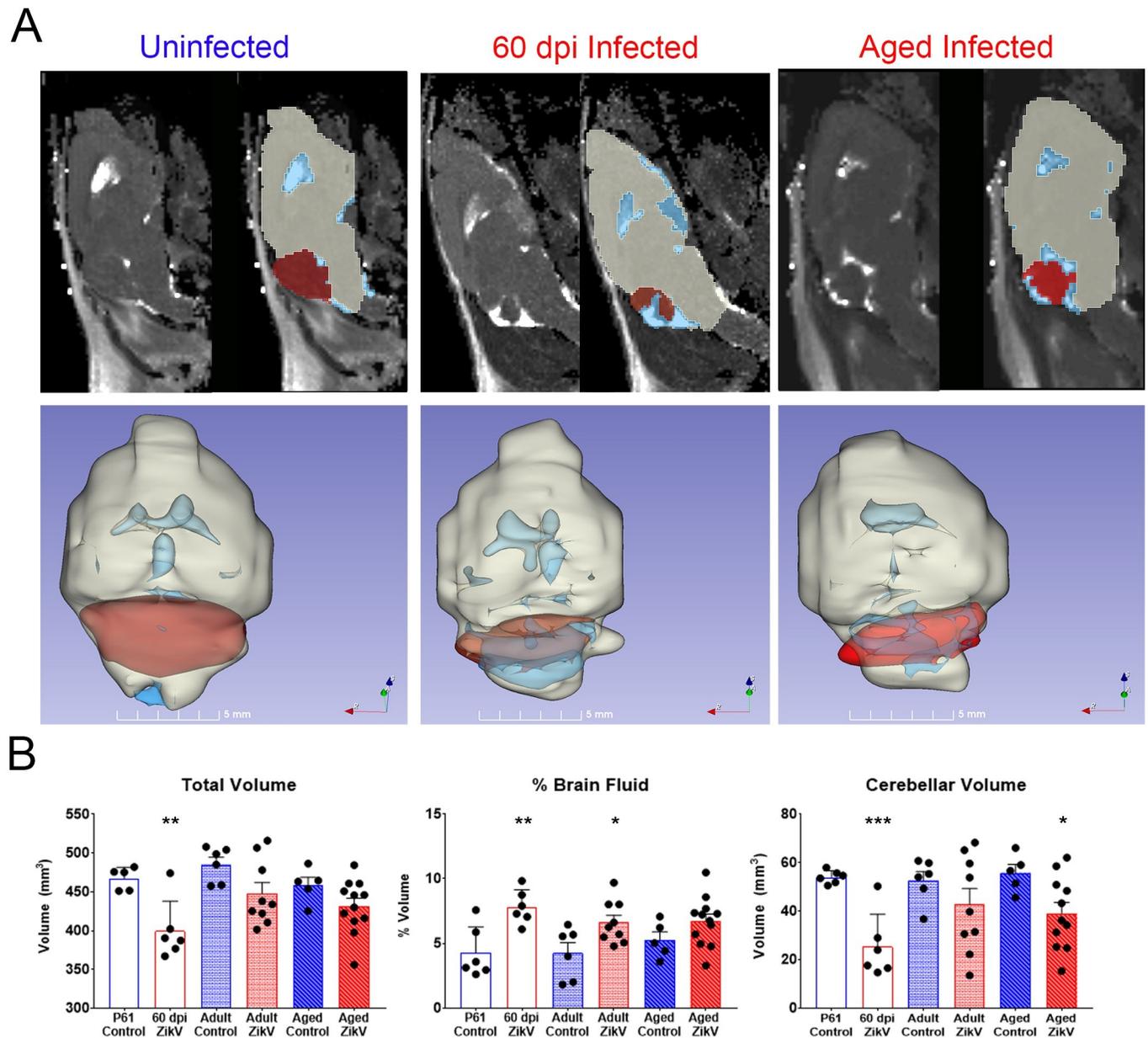
Fig 2. Magnetic Resonance Imaging of ZIKV infected brains. A. representative examples of 2D slices of T2 MRI scans performed on uninfected, 60 dpi and > 1 ypi ZIKV-infected animals. Representative 3D reconstructions of 2D slices, constructed using 3D Slicer software. The cerebellum is in red and fluid in the CNS in blue. **B.** Quantification of MRI for brain volume, % fluid in brain and cerebellum for each age group in the study, as analysed using the 3D Slicer software (N = 6 control, >7 infected mice per time point).

https://doi.org/10.1371/journal.ppat.1008689.g002

Assessment of motility and exploratory behavior using the Open Field Test (OFT) showed that total horizontal motor activity and velocity were increased in ZIKV-infected mice regardless of age, suggesting a hyperactive phenotype (U = 409, *p = 0.005*; Fig 3B). The increased mobility was more pronounced in younger mice (p<0.005), but evident at all stages (p<0.05). Interestingly, while convalescent mice covered more distance in the OFT, they did not spend more time than the control mice in the center of the arena, suggesting that the emotional component of this test was not affected (Figs 3B and S3B). However, ZIKV-infected mice spent

A) Rotarod

B) Open Field Test (OFT)

B) OFT - con't

C) Elevated + Maze (EPM)

D)
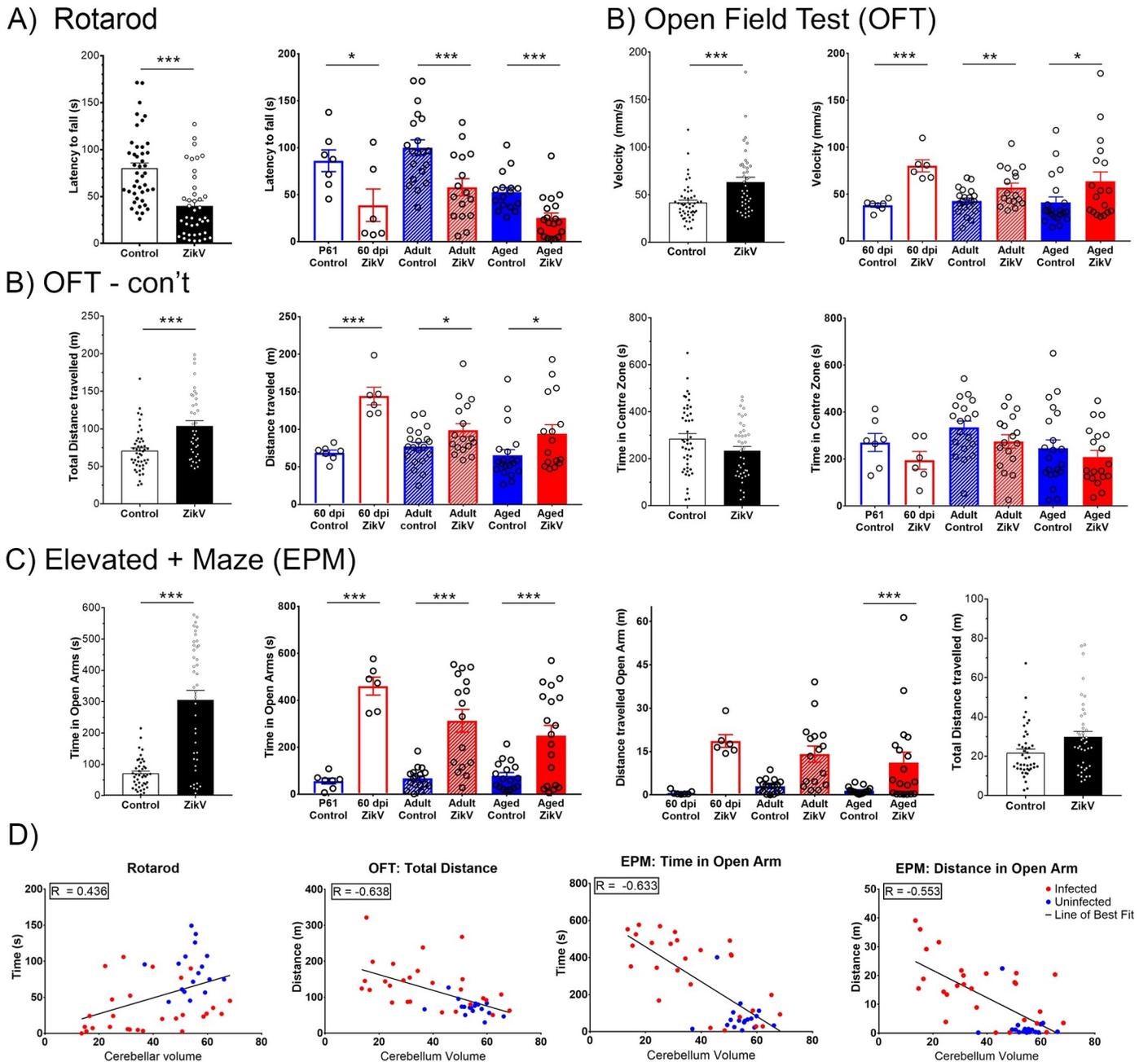
Fig 3. Behavioural studies in convalescent mice. For each test data from infected vs. uninfected mice are shown in black and white bars, while the red and blue bars show the same data parsed by age at the time of testing: young adults (60 dpi); adult (4–8 mpi) and aged (12-14mpi). **A**. Rotarod assay shows time (latency to fall) balancing on a rotating rod of gradually increasing speed over 180 seconds. **B.** Open Field Test (OFT) shows velocity, total distance travelled in the OFT maze and time within the center 20 cm^2 of the maze over a 30-minute period. **C.** Elevated Plus Maze (EPM), explores time and movement in the different areas of the maze. Shown are time spent and distance travelled in the open arm. **D**. **Correlations of performance in behavioral studies and MRI measurements**. See S1 Table for a full list of correlations. Statistical analysis for behavioral studies were conducted using both R (R Core Team (2019) and GraphPad Prism (v. 8.0.1: San Diego, CA). Spearman's rank correlation coefficient was used to correlate MRI and behavior scores. (N = 48 controls, N = 42 ZIKV).

significantly more time (p<0.001) and traveled longer distances on the open arm of the Elevated Plus Maze (EPM) (p<0.001) than on the closed arm when compared to age-matched controls regardless of age (U = 247; *p < 0.0001*) (Figs 3C and S3B). Indeed, a significant

proportion of ZIKV infected mice, across all ages, spent greater than 50% of their time in the open arm, suggesting that ZIKV-convalescent mice have reduced anxiety and thigmotactic tendencies. The overall distance traveled was similar for both groups, indicating that the amount of time and distance travelled in the open arms do not reflect an overall increase in total locomotor activity, but a change in behavioral risk processing. Remarkably, other measures of sociability and learning such as the Social Interaction tests and Novel Object Recognition (S3C and S3D Fig) did not show significant differences between convalescent mice and controls.

Having observed that ZIKV convalescent mice had shorter latency times to fall from the rotarod, displayed hyperactivity in the OFT, and spent more time in the open arms of the EPM ($p \leq 0.001$), we next assessed whether the magnitude of the behavioral changes correlated with the structural changes evident in MRI (Fig 2). As shown in Fig 3E, significant correlations were evident between the brain fluid content and cerebellum volume and latency to fall, as well as between cerebellar volume and the distance travelled in the OFT time or the time and distance traveled in the open arm of the EPM (see full list of correlations in S1 Table). Together, these data indicated that the reduced cerebellar size and increased fluid surrounding the cerebellum of infected animals persists throughout the life of the animals and correlate with motor and behavioral changes.

ZIKV induced neural damage persists long after acute disease

In this infection model, during the acute disease, the virus localizes primarily to the hippocampus, occipital cortex, and most prominently cerebellar cortex. Although the Purkinje cells are not infected, previous studies showed extensive neuronal loss that included Purkinje cells in cerebellum [16]. Since Purkinje cells are critical for the regulation and coordination of motor movement, we next determined whether the infection caused persistent damage to the cellular structure of the cerebellum. Staining of neurons, including GABAergic Purkinje cells, with Neurofilament (NF-H, cocktail of mAb clones SMI-31 and SMI-32) and GAD67 in convalescent mice showed a persistent degradation of the Purkinje cell layer (PCL), both at 60 dpi and 1ypi, throughout the cerebellum (Fig 4A and 4C). In addition, the staining shows an increase in dystrophic and damaged neurites as well as a reduction in the density and complexity of neurites, especially in the molecular layer of the cerebellum of convalescent mice (Fig 4B). This indicated that the cerebellar pathology induced by ZIKV is enduring and could contribute to the motor and coordination defects described above.

Increased cellular infiltration in convalescent mice

As shown above, 30dpi mice had significant reduction in viral load that was associated with fewer infiltrating cells and reduced apoptosis, as well as lower levels of most of the immune-related genes that had been upregulated during the acute infection. This suggested that the infection and associated inflammation was resolving. Despite this, small foci of apoptosis and immune cells in and around the mid-brain, hippocampus and in the granular and molecular layers of the cerebellum were still present at 60 dpi. These foci concentrated in regions that were heavily infected during the acute disease (Figs 1 and S4).

Confocal imaging of the cerebellum, showing TUNEL+ NeuN+ cells indicated that at least some of the cells undergoing apoptosis within these foci were neurons (Figs 5 and S5A). Further, CD45+ immune cells were found in proximity to and within these foci, which were surrounded by GFAP+ astrocytes and rounded Iba-1+ activated microglia (Figs 5 and S5A). Surprisingly, similar apparently active foci of infection could be detected even in aged mice, as shown for the 1-year old mice, although the older mice seem to have fewer NeuN+ cells in the
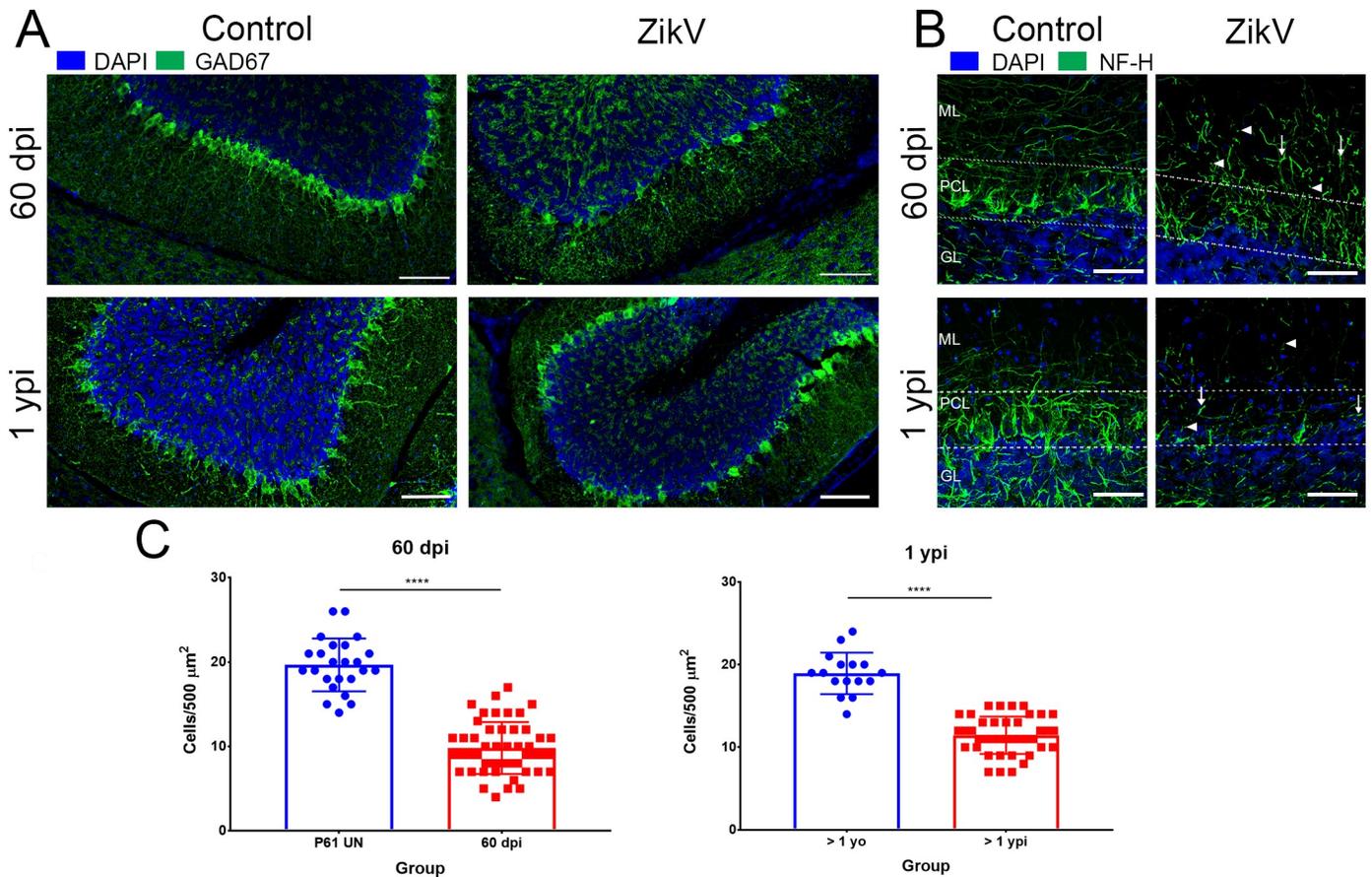
Fig 4. Neuropathology in the cerebellum following neonatal ZIKV infection. A. GAD-67 staining (green) for GABAergic neurons in cerebellum of infected and uninfected controls. Scale Bars = 100 μm. **B.** Confocal imaging of neurofilament heavy chain (NF-H, green) staining in cerebellum. Images are maximum intensity projections of at least 16 Z-planes through each section. ML = molecular layer, PCL = Purkinje cell layer, GL = Granular Layer. White arrows indicate dystrophic neurites, white arrowheads indicate interrupted neurites. Scale Bar = 50 μm. **C.** Quantification of Pukinje cells at 60 dpi and 1 ypi. The mean number of cells in 500 x 500 μm regions centered on the Purkinje cell layer. 8 ROI per cerebellum, centering on GAD-67 stained PCL was quantified using Olympus VS software, ver 2.9. Dots represent number of cells in an ROI. Bars represent the mean quantification. Data is presented as a mean of the number of cells in all ROI counted (N = 3 uninfected. 4 infected from 2 independent experiments). (Mann Whitney test p<0.001).

center of the foci. Of note, while the microglia immediately surrounding the foci have hypertrophic bodies and asymmetric processes, indicating activation, those that are distant to these apoptotic foci are in a resting state, with small soma and long, complex processes, suggesting that the areas of inflammation are very localized (Figs 5 and S5B). Together, this showed and enduring localized, active inflammatory processes in the brains of convalescent mice.

Persistent inflammatory gene expression in CNS of ZIKV-exposed animals

Acute meningoencephalitis due to ZIKV was associated with the up-regulation of the expression of genes linked to interferon responses, recruitment and activation of macrophages, and neutrophils, inflammation, as well as genes corresponding to infiltrating T cells (Fig 1D). To investigate whether the small foci of infiltrating cells and activated microglia were associated with an increase in the expression of immune-related genes, we examined the mRNA expression level for a panel of immune-related genes in cerebellum and cerebrum of convalescent mice at 2, 4–6 and 12–14 mpi (Fig 6). Surprisingly, while the relative expression levels were lower than during acute infection, the brains of convalescent animals showed a similar pattern
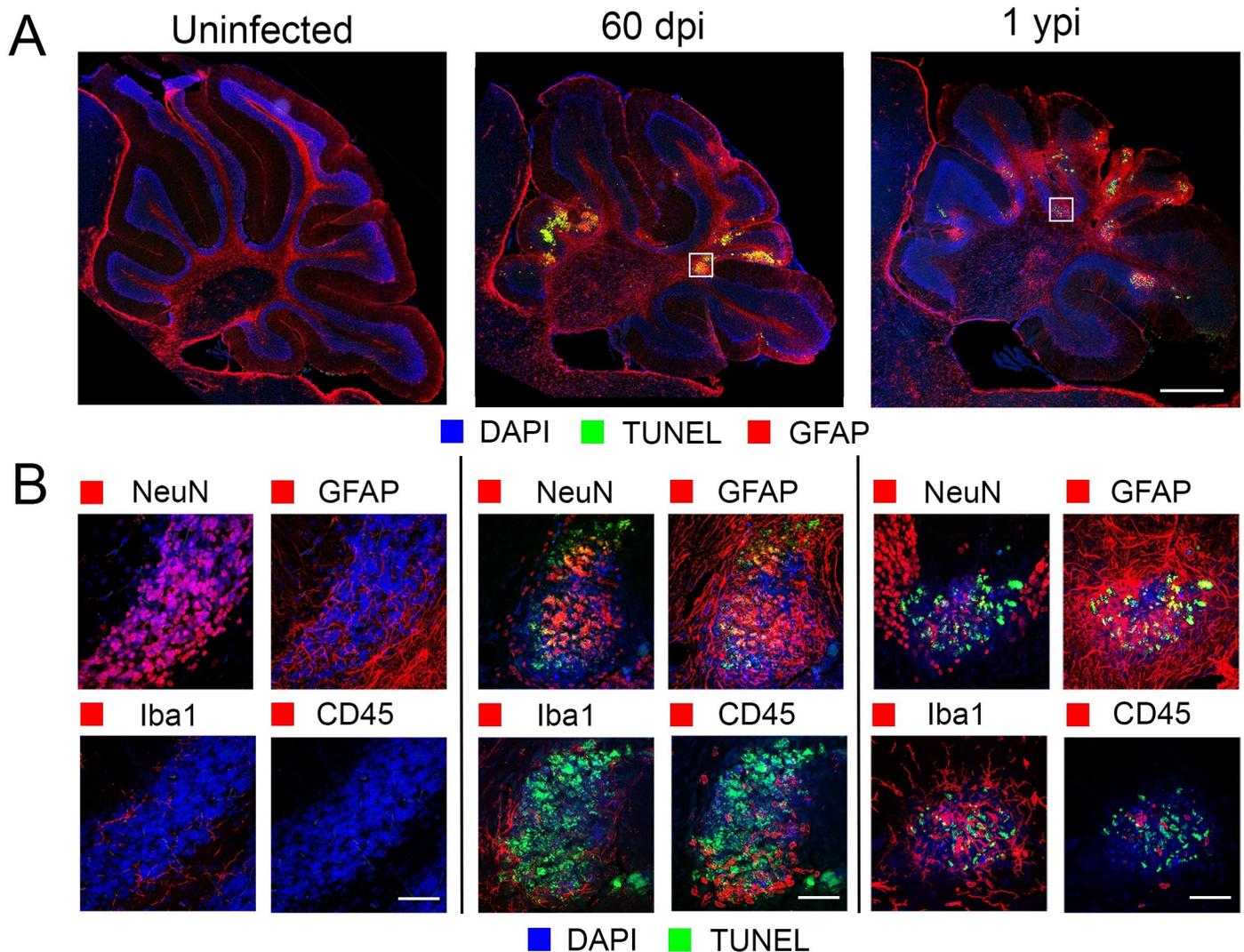
Fig 5. Apoptotic foci in cerebellum of ZIKV infected animals. A. IHC staining of cerebellum of infected mice 60 dpi and 1ypi shows apoptotic foci (TUNEL⁺, green; DAPI, blue) surrounded by activated astrocytes (GFAP⁺, red). Scale Bar = 500 μm. **B**. Confocal microscopy of these lesions indicates apoptotic cells (TUNEL+, green and DAPI, blue in all images), surrounded by activated astrocytes (GFAP+, red) with activated microglia (Iba-1, red) and infiltrating immune cells (CD45+, red) proximal to and within the lesions. Scale Bars = 50 μm.

of gene expression with increased levels of interferon-stimulated genes such as *Cxcl10*, *Cxcl11*, and *Oas1* in convalescent mice. The expression of genes linked to macrophage/microglial activation including: *H2-Eb1*, *Cd40*, *Cd68*, *Cd80*, and *Cd86*, as well as *C3*, *Il6* and *Tnf* were also increased, regardless of age. In addition, a marked increase in chemokine expression, particularly *Ccl2* and *Ccl5*, as well as pro-inflammatory cytokines *Ifnγ* and *Il1α* was evident at all ages. Lastly, in accordance with the increased CD45⁺ cells shown by IHC (Figs 5, S4 and S5), there were increased levels of *Cd3*, *Cd8a*, *Ctla4*, *Gzmb*, *Icos* and *Gitr*, suggesting the presence of residual or bystander CD8+ T cells in the tissue and confirming the presence of active inflammatory processes in the CNS months after the challenge. Interestingly, the increased levels of mRNA were detectable not only in cerebellum, where the foci are located, but also in cerebral cortex suggesting that many areas of the parenchyma are exposed to increased inflammatory signals long after initial infection.
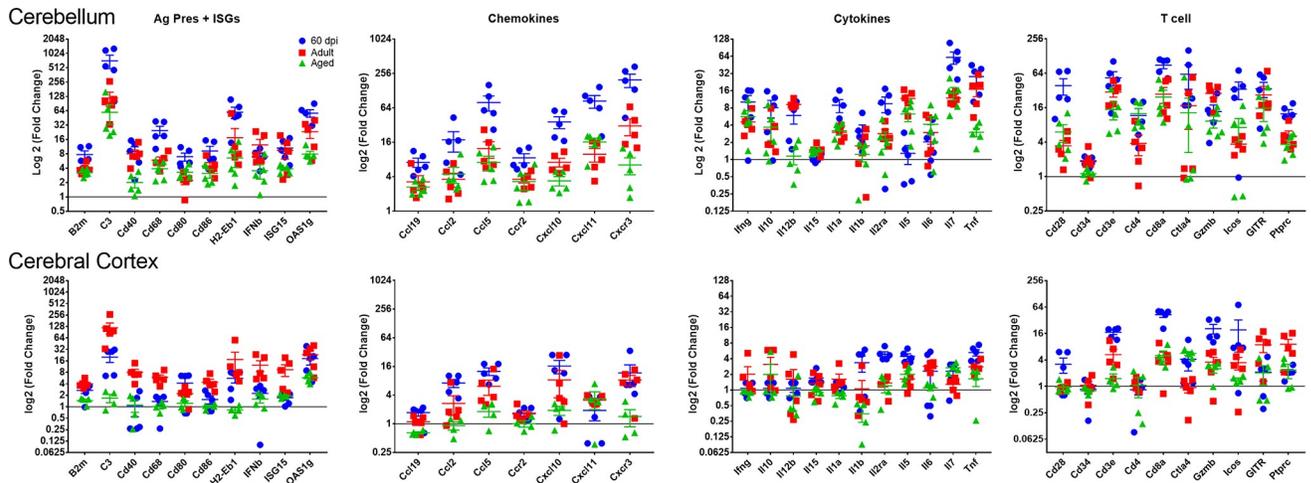
Fig 6. Expression of immune-related genes in the CNS of ZIKV infected animals. Cerebellum and cerebral cortex were isolated from the CNS of 60-day (blue symbols), adult (4–8 mo., red symbols) and aged (> 1y, green symbols) ZIKV-infected animals and gene expression analysed by real-time PCR using Mouse Inflammation Taqman array cards (Thermo Scientific). Genes associated with antigen presentation (Ag Pres) and IFN-inducible genes (ISG); T cell function; chemokines and pro-inflammatory cytokines; were grouped together. Ct values analysed using Quant-studio software (Thermo Scientific) using relative threshold algorithm for analysis. Data is presented as normalized against house-keeping genes and fold-change over age-matched, mock-infected controls as calculated with the ΔΔCt method.

Testing gene expression in the subgroup of mice that had undergone the MRI and behavioral testing allowed us to correlate the expression of pro-inflammatory genes with the behavioral sequelae in individual mice. The distance covered in OFT as well as the time and distance covered in the open arm of the EPM correlated with the mRNA levels in cerebellum for pro-inflammatory genes including *Cd80*, *Cd86*, MHC, and *Cd68*, ISGs *Cxcl10*, *Cxcl11*, and *Stat1*, and pro-inflammatory markers *C3*, *Csf1*, *Il-1α*, *Il-18*. In addition, cerebellum size correlated with the expression levels of *Ifnγ*, *Tbet*, *Stat1*, *Stat4*, *Prf1 and Gzmb* suggesting an association with Th1 linked responses, while changes to the ratio of social to non-social interaction correlated with levels of *Il-14 (r>0.7)* and *Il-13 (r = 0.48)* in cortex. In addition, reduced latency to fall in the rotarod correlated with increased expression of *Tbet*, *Icos* and *Cd4*, although not *Cd8* (S2 Table). Chronic inflammatory processes in CNS have been associated with Parkinson's, Alzheimer's, and other neurodegenerative diseases of aging. Future studies will need to explore the extent to which the protracted inflammatory process contributes to the motor and behavioral deficiencies and whether it could predispose convalescent patients to neurodegenerative diseases later in life.

ZIKV RNA, ZIKV antigen, and infectious ZIKV persists in the CNS of neonatally infected animals

Initial experiments using TCID$_{50}$ assay on homogenates from the hemispheres of infected animals were negative after 22 dpi suggesting that infectious ZIKV had been cleared from the CNS. Further, staining with human polyclonal antibody or mouse monoclonal antibody specific for the E-protein for ZIKV antigen showed vestigial viral antigen in the cerebellum by 30 dpi (Fig 1) and no positive staining in cerebellum or other regions of the brains of exposed mice by 60 dpi (not shown). However, the persistent inflammatory gene expression, including type 1 IFN and ISGs, as well as the ongoing apoptosis, infiltration of immune cells and gliosis occurring at foci within the cerebellum of adult animals suggested that low levels of virus, below the level of detection of two-step IHC, could persist in the CNS of neonatally infected
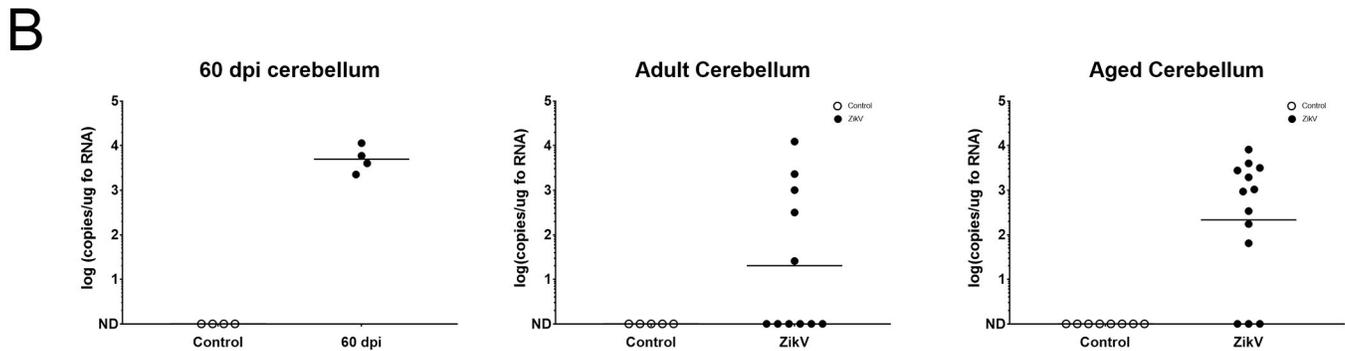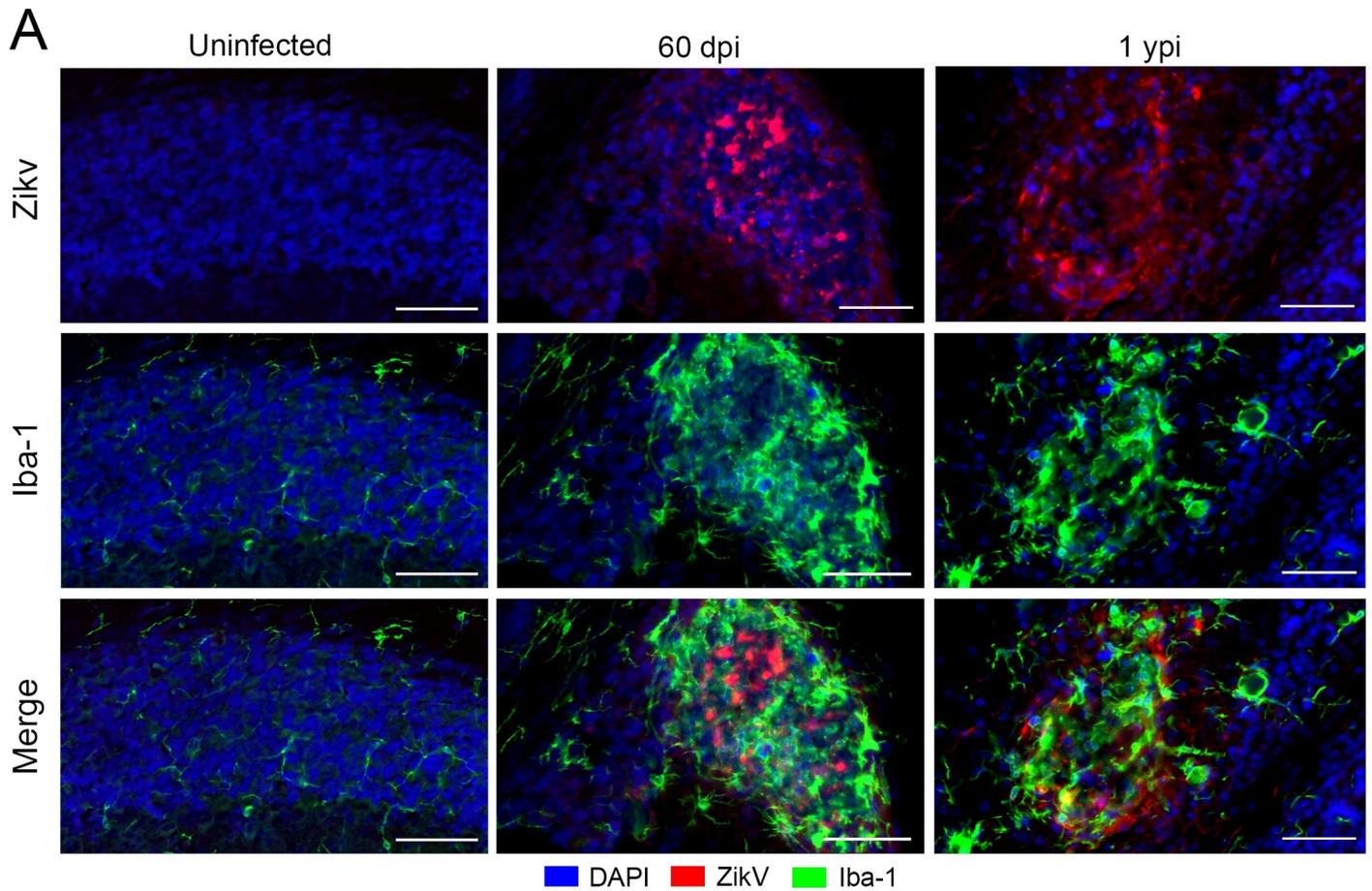
Fig 7. ZIKV antigen and RNA persistence within cerebellar lesions. A. IF-IHC using Tyramide Signal amplification in combination with anti-ZIKV E protein (red, top) identifies virus antigen within cerebellar lesion at 60 dpi and 1 ypi. Note the hypertrophied nuclei of activated Iba+ microglia (green) surrounding the viral antigen (bottom, merge). Scale Bars = 50 um. **B.** Real-time PCR for viral genome in cerebellum at 60 dpi, 4–8 mpi and 12-14mpi.

https://doi.org/10.1371/journal.ppat.1008689.g007

animals. To address this, we amplified the IF-IHC signalling using a multi-step technique with hyper-peroxidase labelled, secondary antibodies combined with a fluorescent HRP substrate, to improve the detection of residual ZIKV antigen. As shown in Fig 7A, viral antigen was evident within foci of the granular layer (as marked by activated microglia) of the cerebellum at both 60 dpi and 1 ypi suggesting that the inflammatory processes surrounded the residual viral antigen. Images of the entire cerebellum, which confirm the specificity of the high-sensitivity staining and the proximity of activated microglia to virally infected cells are available in S6 Fig.

To determine whether the viral antigen was associated with viral RNA, we next tested the tissue for viral RNA using a one-step RT-qPCR, with primer/probes specific to detect ZIKV. This showed the presence of viral genome RNA (positive-sense) in the brains of mice at 60 days 4 to 6 months, and 1-year post infection in 40–60% of convalescent mice (Figs 7B and S7). ZIKV expression levels appeared higher in cerebellum (10^3–10^5 copies of viral RNA/ug total RNA) than cortex (S7 Fig, 10^1–10^3 copies of viral RNA/ug total RNA). To confirm that the RNA detected was not residual but represented replicating virus, we next selected the brains that had positive-sense ZIKV RNA and tested them for the presence of negative-sense RNA strands. Negative-sense RNA is considered indicative of ongoing replication as it is a replicative intermediate of positive-sense RNA viruses and typically has a very short-half life. All the mice with quantifiable levels of viral RNA (positive-sense strand) showed detectable levels of negative-sense strand RNA, confirming the presence of replicating virus (Fig 8A). Lastly, we examined whether the detectable virus in convalescent adults was infectious by seeding brain homogenates on VERO cells, which after 5–7 days were fixed and stained with anti-ZIKV E-protein. As shown in Fig 8B, VERO E6 cells exposed to the cerebellar homogenates of mice older than 1 ypi, replicate ZIKV indicating infection of these cells by virus. This confirmed that ZIKV can establish a persistent reservoir in the CNS of mice challenged early in development.

Discussion

These data were collected from immune competent mice exposed systemically to ZIKV peri-natally, to explore the acute and long-term neurodevelopmental impact of perinatal Zika infection. It shows that a peripheral (subcutaneous) challenge with ZIKV shortly after birth causes a meningoencephalitis characterized by the infection of neurons in cerebellum, hippocampus, and the cerebral cortex that is associated with extensive apoptosis and immune cell infiltration, as well as reduced number of Purkinje cells and other GABAergic and granular neurons. The severe ataxia and dystonia that are evident during the acute infection subside within 30 days of challenge, and the animals appear to recover without overt motor or behavioral deficiencies. However closer examination, pairing MRI scans, behavioral testing, and gene expression studies shows that convalescent mice have reduced cerebellar volume and the magnitude of the defect correlates with deficits in motor coordination, hyperactivity, and impulsive or risky behavior that are evident even in aged mice. Further, we show that while the most severe tissue damage appears to occur during acute infection, the brain parenchyma in convalescent mice harbors low levels of replicating virus localized in small foci with active apoptotic processes and cellular infiltrates that are surrounded by activated astrocytes and microglia. The lesions are associated with a pattern of gene expression that indicates a continuous inflammatory milieu as late as a year post-infection. Together, these studies raise the possibility that virus may also persist in patients leading to chronic local inflammation and apoptosis. This suggests that the use of anti-viral drugs to completely eradicate the virus from the brain man be considered, and that anti-inflammatory or immunosuppressive therapies in patients that were infected with Zika early in life should be undertaken with caution. Further, the data suggests the need to closely monitor exposed children, as an apparently transient ZIKV infection early in development could result in life-term behavioral and psychological deficits. Lastly, our studies provide a platform to investigate the host-pathogen interactions in steady-state within the CNS as well as test therapeutics to clear ZIKV from the CNS and/or to mitigate damage caused by the associated chronic inflammation.

The most severe cases of CZS can include severe malformations of the brain (microcephaly, simplified gyral pattern, cerebellar hypoplasia, calcifications, ventriculomegaly), eyes
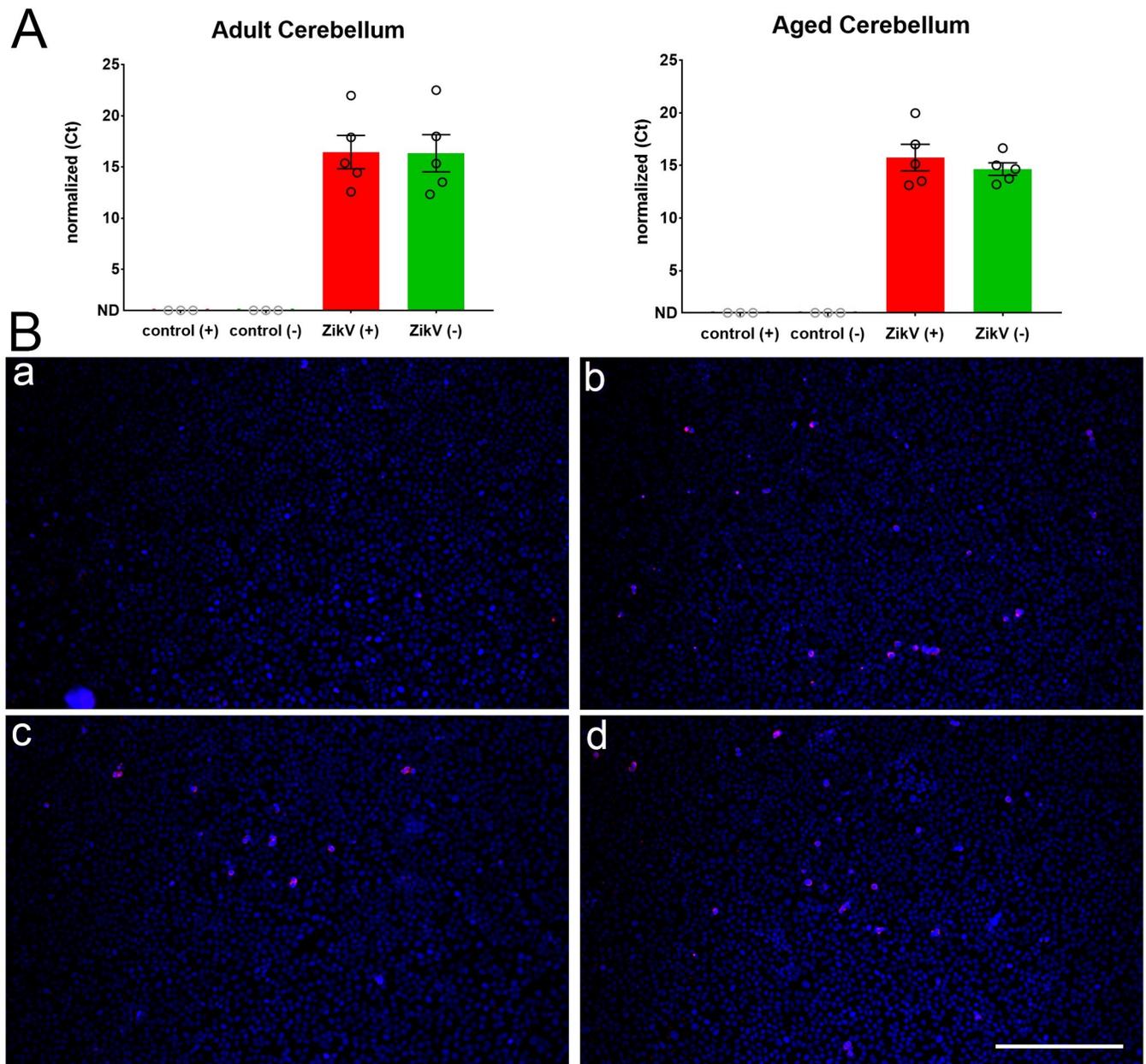
Fig 8. Evidence of live ZIKV infection in adult and aged brains. A. The RNA from brains of mice that were ZIKV+ (Fig 7) was tested for the expression of ZIKV-positive RNA (red bar) and -negative sense RNA (green bar) in the cerebellum. Controls include uninfected age-matched animals > 1 year old. Ct values normalized to housekeeping gene (GAPDH). ND = no detectable amplification after 40 cycles. **B**. Infection of Vero E6 cells with cerebellar homogenate from (a) cerebellum (Cbx) homogenate from uninfected, aged-matched control mice, (b) ZIKV PRVABC059-infected positive control (0.01 MOI), (c/d) cerebellar (Cbx) homogenate from each of 2 ZIKV-infected mice at > 1 ypi. All cultures were stained with mouse monoclonal anti-ZIKV E-protein antibody and counterstained with DAPI to mark cell nuclei. Scale Bar (for all images) = 100μm.

(microphthalmia), and limbs and are diagnosed in 5–10% of children exposed *in utero* early in pregnancy. Further, there is mounting evidence that some infants exposed to the virus who do not exhibit CZS at birth, develop neurodevelopmental abnormalities such as hydrocephalus, or severe hearing and ocular defects later in life [27]. Indeed, while initially ZIKV was thought to be neurotropic only in early pregnancy, recent studies demonstrate astrogliosis, multifocal meningeal lesions, and altered neurodevelopmental processes in late pregnancy and even in

infants, which is not surprising given that synapse formation, pruning and myelination processes extend for years after birth [28,29]. Further, recent *in vitro* studies show that while the virus preferentially infects immature progenitors, it can replicate in mature neurons [21, 30]. Together, this raised concerns that, in addition to the expected sequelae of severe malformations due to early ZIKV infection, perinatal exposure to ZIKV, even if apparently asymptomatic, can cause subtle changes in neuronal maturation and neuroplasticity leading to motor, behavioral, learning, or psychiatric difficulties that may become evident years after exposure [27].

Developmentally, the CNS of mice at P1-3, like humans in week 23–32 of pregnancy, are undergoing extensive neurite outgrowth and synaptogenesis, have pre-oligodendrocyte progenitor cells that are actively undergoing proliferation, and a BBB that is established but not fully mature [31]. ZIKV challenge at this time resulted in infection of glutamic acid decarboxylase (GAD67+) neurons in the hippocampus, cerebral cortex, and most prominently the molecular layer of the cerebellar cortex [16,20] with extensive neuronal loss. Correlation of the anatomical sequelae as detected by MRI, with histopathological changes and immunological responses for over 1 year shows that mice do not develop microcephaly or obvious calcifications or increased lateral ventriculomegaly. Increased fluid volume in the CNS, particularly in and around fourth ventricle and pia layers of the cerebellum and reduction in cerebellar size where most apoptotic lesions are also located during acute infection, are indicative of persistent changes to the microstructural composition of the tissue in this region. Importantly, the magnitude of the reduction in cerebellar volume correlated not only with the reduced latency to fall on the rotarod, but with the degree of hyperactivity and impulsivity. The results parallel a previous study conducted by Snyder-Kelley *et al* using young adult mice (60dpi) in a similar model and extend the observations to adult and aged mice demonstrating that although the virus retracts over the first 60 dpi, the neurological sequelae are long-term [32]. Of note, increased fluid and/or disruptions in fluid diffusion in CNS have been described in patients with multiple neurologic and psychiatric disorders including children exposed in utero to HIV [33]; future studies using higher resolution MRI in convalescent patients may provide some insight into ZIKV-induced defects in infected children.

Immune responses in the CNS infection require a delicate balance between efficient pathogen clearance and the preservation of sensitive, non-renewable neural cells [34,35]. During acute ZIKV infection, the majority of CD45+ infiltrating cells are T cells, particularly CD8+, which have been shown to play a key role in viral clearance, and mice with defective T cell responses succumb to infection [16,20,36]. However, T cells can mediate tissue destruction and excessive inflammation [37]. Importantly, previous studies have reported the long-term persistence of pathogen-specific resident memory CD8+ T cells in CNS that adopt a quiescent state [38–40]. In this model however, the presence of apoptotic cells including apoptotic neurons, and a pattern of gene expression that suggest the presence of activated microglia/macrophage (*C3*, *Tnf*, *Ccl5*, *Cxcl10*), ongoing antigen presentation (*β2m*, *H2-Eb1*, *Cd86*), and activated T cells (*Cd3ε*, *Cd8*, *Cd4*, *Ifnγ*, *GrzmB*, *Prf1*, but not *Ctla4* or *Pd1*) as late as a year post infection suggests that the cells infiltrating these foci are not quiescent, but actively responding and possibly controlling the infection. Indeed, our preliminary studies suggest that the T cells that can be found in the CNS at 1ypi, adopt the phenotype of CD8+ resident effector memory cells. Future studies will be needed to fully characterize the T cells that persist in CNS as these could contribute to the pro-inflammatory milieu and worsen the neurological damage [41,42]. Indeed, while the lytic effect of the virus during acute infection is likely the predominant determinant of the persistent lesions and behavioral changes, the presence of proinflammatory cytokine and chemokines may impair healing and continue to skew the formation and pruning of synapses contributing to the motor and behavioral defects observed[43]. This could

increase the risk of neurodegenerative conditions including Alzheimer's, Parkinson's, and multiple sclerosis over time [40,44].

Many neurotropic viruses have been shown to persist in CNS, and in some cases can lead to recrudescence later in life [35]. The nonlytic cellular mechanisms that govern viral latency and reactivation of DNA viruses, such as HSV and VZV, are reasonably well understood, however less is known about the persistence of RNA viruses in the CNS [22]. Detectable levels of genomic RNA in the mouse brain parenchyma has been described for West Nile, Sindbis, Lymphocytic choriomeningitis, Borna disease virus, rabies virus, and influenza A virus suggesting that RNA viruses can establish long-term quiescent infection in CNS neurons but persistence of infectious flaviviruses in CNS has not been previously demonstrated [35,45]. Unlike those viruses, ZIKV appears to remain replication-competent, albeit at levels far below those of the peak infection and confined to complex structures that are surrounded by activated microglia and astrocytes. Whether these cells contain the replicating virus impeding its spread or reflect a localized response to the low level of apoptosis induced by the virus remains unknown. The IHC imaging of the CNS foci in adult mice suggest that at least some of the neurons are infected by the virus, however the density of neurons within the foci appears to diminish over time. Thus, while long-lived CNS neurons may be an ideal harbor for long-term infection, the staining suggests that other cells may be involved as well. Future studies will need to examine: 1) whether anti-inflammatory treatments can destabilize apparent stalemate between the virus and the surrounding activate microglia; 2) whether these discrete foci of inflammation increase the risk of neurodegenerative diseases; and 3) the degree to which the inflammatory barrier that contains the virus can hinder the use of antivirals to eliminate the infection.

A critical question stemming from the discovery that live virus persists in the CNS, is whether it contributes to the motor and behavioral defects. While our studies show that mice that survive an infection with ZIKV early in life develop enduring defects in their motor skills and altered behavior, the deficiencies do not appear to worsen with age, suggesting that the tissue damage that occurs during the acute disease is the main determinant of the clinical phenotype, however the contribution of the pro-inflammatory milieu to the persistence of symptoms is still unknown. Given the potential plasticity of the brain early in life, future studies will need to explore whether eradicating the virus from the CNS and avoiding the protracted exposure to a proinflammatory milieu allows for a better reconstitution of the tissue. Conversely, as the foci of virus are surrounded by activated glia, it is possible that exposure to immunosuppressive or anti-inflammatory therapies such as TNF inhibitors could limit the tissue damage, but could also facilitate the spread of the virus [46,47]. or induce recrudescence of the virus in the CNS as has been observed with neurotropic coronavirus JHM [48,49]. Our preliminary studies treating chronically infected mice with cyclosporin or dexamethasone to suppress the immune response in ZIKV did not result in increased mortality. Future studies will need to explore the impact of therapeutic immune modulators on viral load and sequelae.

In summary, these studies confirm that mild perinatal infections can results in long-term neurological sequelae and concordant persistent behavioral deficits of the host. Further, they provide a new understanding of the potential impact of ZIKV infections of the CNS by demonstrating that convalescent mice harbor multiple small foci with viral antigen, active apoptotic processes in neurons, and cellular infiltrates that appear to be walled-in by activated astrocytes and microglia as late as 1-year post-infection. The detection of negative strand viral RNA in addition to the genome, and recovery of infectious virus from the brain of convalescent mice demonstrates for the first time that ZIKV can establish a persistent reservoir in the CNS. The model described herein opens a novel opportunity to understand the role of the host immune response in active containment of the virus within the CNS and provides a platform to

examine the role of the host immune response in active containment of the virus within the CNS and understand what circumstances could lead to viral recrudescence.

Materials and methods

Ethics statement

All experiments in this manuscript were completed with the approval of the WO Consolidated Animal Care and Use Committee (ACUC) under the approved Animal Study Proposal 2019–02. The use of Zika virus was approved under the White Oak Institutional Biosafety Committee (IBC) under approved Application 11420.

Mice

C57BL/6 (B6) mice used in this study were bred and housed in sterile microisolator cages under 12-hour day/night cycle. They were given food and water ad libitum in the specific path-ogen-free, AAALAC accredited animal facility of the U.S. Food and Drug Administration's (USFDA) Division of Veterinary Medicine (Silver Spring, MD). This study was carried out in strict accordance with the recommendations in the NIH guide for the Humane care and Use of Laboratory Animals and with the approval of the White Oak Consolidated Animal Use and Care Committee at US-FDA.

Zika virus PRVABC59 (ZIKV) preparation

Zika virus PRVABC59 (Puerto Rico strain) used in this study is a contemporary strain that was isolated by the CDC from the serum of a ZIKV infected patient who travelled to Puerto Rico in 2015. The complete genome sequence is published (Ref. Gene bank accession # KU501215). Virus stocks from the CDC were kindly provided by Maria Rios (USFDA). This virus stock was expanded in Vero E6 cells. Briefly, cells were inoculated with the CDC pro-vided stock for 1 hour at 37˚C, then provided growth media and incubated for 5–7 days at 37˚C, 5% CO_2. Supernatants were collected, clarified by centrifugation (10000 x g, 10 min) and the titer of the stock determined by $TCID_{50}$ assay as previously described [50].

ZIKV infection and organ collection

All newborn mice were inoculated with 2000^*TCID_{50} of ZIKV, in 10 µl by subcutaneous (s.c.) injection with a 31G needle at the scruff of the neck. C57BL/6 mice (sex indeterminant) were inoculated one day after birth (P1). Control animals were injected (s.c.) with the same volume of diluent (MEM). All littermates received the same treatment in order to avoid cross-contami-nation. At the indicated time post-infection, mice were euthanized by CO_2 asphyxiation and exsanguinated by transcardiac perfusion with ice-cold PBS prior to collecting the brains. For some studies, brains were bisected sagittally prior to freezing. Mice were weaned 21 days after birth and housed with same-sex littermates (2–5 mice per cage).

Virus quantification by real-time qPCR

One microgram (µg) of isolated total RNA from infected and age-matched uninfected controls (procedure described below) was analyzed to establish ZIKV RNA levels, which are expressed as ZIKV copies/µg. Absolute quantification was determined using genomic viral RNA tran-scribed from a plasmid using the T7 Megascript transcription kit (ThermoFisher). The number of copies was calculated based on absorbance at 260 nm. One-step reverse transcription (RT)-real time qPCR was performed on a 10-fold serial dilution of this standard RNA in parallel with 1 µg of unknown sample RNA. This assay amplifies ZIKV genome position 1087 to 1163 based

on ZIKV MR 766 strain (GenBank accession no. AY632535) Zika virus RNA transcript levels in the samples [51], in a single tube using a 25 μl reaction volume (RNA to cDNA kit, Thermo-Fisher). Reaction parameters for the Applied Biosystems Viia7 real time PCR machine: 60˚C for 30 min for reverse transcription, followed by 95˚C for 15 min to inactivate the RT enzyme and activate the DNA polymerase followed by 45 cycles of 95˚C, 15 sec and 60˚C for 1 min.

Detection of positive-and negative-sense strands of ZIKV was performed as previous described [52] in a 2-step real-time PCR reaction. Briefly, reverse transcription of total RNA isolated from brain or infected Vero cells was performed using T7- or GVA-tagged, ZIKV-specific primers and Oligo d(T)$_{16}$ primers (ThermoFisher, Carlsbad, CA) for first-strand synthesis (High Capacity cDNA reverse transcription kit (ThermoFisher Scientific, Carlsbad, CA). These reactions synthesized T7-tagged positive-sense and GVA-tagged negative-sense viral cDNA. The resulting cDNA was amplified using qPCR with forward primers binding to the strand-specific Tags (T7 or GVA) and reserve primers were specific to the ZIKV E gene sequences. A common Taqman probe specific for the ZIKV amplicon was used to detect amplified cDNA. All custom primer/probes in this assay were produced using sequences previously described [52] and produced by Eurofins Genomics, USA. As no standard curve was available for both strands, relative levels of the transcripts are expressed here.

Taqman low density array for gene expression

Flash-frozen brains (half brains bisected along the longitudinal fissure) were homogenized in 1 mL Trizol reagent (ThermoFisher, Carlsbad, CA) using a Precellys-24 (Bertin Instruments) equipped with a Cryolys cooling unit, with 1 mm Zirconia beads (BioSpec Products). RNA was isolated following the manufacturers' protocol and resuspended in ultra-pure ddH$_2$O. The concentration and purity of isolated RNA was determined by spectrophotometry at 260 nm and 280 nm using a NanoDrop spectrophotometer (ThermoFisher, Carlsbad, CA). To eliminate potential genomic DNA contamination, the DNA-free Turbo kit (ThermoFisher, Carlsbad, CA) was used as per the manufacturer's protocol. Reverse transcription was performed on 1 μg of total RNA, using Multiscript High Capacity Reverse Transcriptase (ThermoFisher, Carlsbad, CA), per the manufacturer's protocol, using random primers. The resulting cDNA was diluted ten-fold with ultra-pure, nuclease-free water and stored at -20˚C prior to use in real-time Taqman PCR reactions (ThermoFisher, Carlsbad, CA). The resulting cDNA was loaded into a Mouse Inflammation array card (ThermoFisher, Carlsbad, CA) and real-time qPCR was performed using a Viia7 real-time PCR instrument. All fold-change calculations were performed using the ΔΔCt method [53], normalizing against GAPDH and age-matched uninfected controls.

Nanostring analysis of gene expression

Mouse Immunology Panel (v2) (Nanostring Technologies, Seattle, WA) Reporter and Capture probes were mixed with 100 ng of total RNA (20 ng/μl in molecular grade, ultra-pure ddH$_2$O) isolated from the CNS of uninfected and ZIKV infected animals. The hybridized probe/samples were then processed, and data acquired using the Nanostring MAX acquisition system, counting 280 fields of view (FOV) per sample. These data were normalized to internal controls and housekeeping genes in the panel. Gene expression is expressed as fold change in gene expression relative to age-matched, mock-infected control animals. The data was analyzed using Nanostring nSolver (ver. 4) and plotted using GraphPad Prism (ver 7).

Immunofluorescence Immunohistochemistry (IF-IHC) and histology

Brain halves from ZIKV-infected and age-matched uninfected control were placed in freshly prepared 4% paraformaldehyde (PFA) solution (in 1 x PBS pH 7.4) immediately after

extraction. After 24 hours of fixation at 4˚C, the tissue was transferred to 30% sucrose in 1 x PBS for cryoprotection. The brains remained in 30% sucrose at 4˚C until they sank in the solution (typically ≥ 24 hours). Sucrose embedded tissue was mounted in TissueTek O.C.T (Sakura-Finetek, Torrance, CA) and frozen. The brains were stored at -80˚C until sectioned. Sagittal sections (25 μm thick) were cut using a Leica CM1900 cryostat at a chamber temperature of -20˚C (Leica Biosystems, Buffalo Grove, IL) and mounted onto Superfrost-Plus Gold microscope slides (Fisher Scientific, Carlsbad, CA). Mounted sections were stored at -20˚C until staining. Prior to staining, sections were warmed to room temperature (RT) to dry, then immersed in phosphate buffered saline (PBS). For antigen retrieval, the sections were immersed in 0.1M Sodium Citrate solution, pH 8.5 at 80˚C for 8 minutes, then allowed to cool at room temperature for an additional 10 minutes. The sections were then washed with PBS and permeabilized using 0.5% Triton X-100 in PBS for 60 minutes at RT. The sections were then blocked with 5% normal goat serum and 1% bovine serum albumin (BSA) in PBS + 0.5% Triton X-100 for 2 hours. Primary antibodies used include: human polyclonal anti-Zika virus antibody (Kerafast EVU302, MA) or mouse anti-ZIKV E protein mAb (Fitzgerald, 2713), neurofilament heavy chain cocktail (SMI31 and SMI32 mAb, Biolegend), rat anti-CD45 (BD Biosciences), rabbit anti-Ionized calcium-Binding Adapter molecule-1 (Iba-1) (Wako), rabbit anti-glial acidic fibrillary protein (GFAP)(Dako), mouse anti-glutamic acid decarboxylase 67 (GAD67) (SigmaMillipore). Tissue sections were incubated overnight in a humidified chamber at room temperature with primary antibodies diluted with 1% BSA in PBS + 0.5% Triton X-100. The slides were then washed with PBS + 0.05% Triton X-100 followed by 1 x PBS and treated with the appropriate AlexaFluor (AF)-conjugated secondary antibodies (raised in goat) (ThermoFisher, Carlsbad, CA), diluted in 1% BSA in PBS + 0.05% Triton X-100 for > 120 min at RT. To increase sensitivity of the staining assay, we used the AlexaFluor 647 Tyramide Superboost (goat anti-rabbit) kit (ThermoFisher, Carlsbad, CA) as per the manufacturers' protocol for detection of anti-ZIKV E protein. *Quantification of Purkinje cells*. For both ZIKV-infected and uninfected, age-matched controls, the cerebellum of GAD-67 stained sections were marked with 8 regions of interest (ROI) (500 x 500 μm), centering on the Purkinje cell layer. The number of Purkinje cells in each ROI was quantified.

Staining for apoptosis was performed using the TUNEL assay (ApopTag-FITC, SigmaMillipore) preceded by antigen retrieval (as described above) as per manufacturer's instructions. All IF-IHC sections were mounted with Pro-Long Diamond anti-fade mounting media containing DAPI (ThermoFisher, Carlsbad, CA). AF-labelled antibodies were detected at emission wavelengths: 405 nm (DAPI), 535 nm (Alexa-fluor 488), 605 nm (Alexa-fluor 568) and 650 nm (Alexa-fluor 647). Sections were imaged using an Olympus VS-120 virtual slide microscope (Olympus LSS) using a 20x or 40x objective lens. Regions of interest were captured using VS-Desktop software (ver 2.9, Olympus LSS). For confocal imaging, images were acquired using a Zeiss LSM 880 confocal microscope, using 405 nm (DAPI), 488 nm (AF488), 561 nm (AF568) and 633 nm (AF647) excitation lasers. Optimal fluorescence detection settings were determined and applied to all sections equally. Images were acquired using the Zeiss Zen software. Maximum intensity projections of acquired Z-stacks were compiled using Zeiss Zen and/ or ImageJ + Fiji (NIH) software [54]. *For identification of virus infection in Vero cells*: After adsorption with ZIKV for 2 hours, cells were washed and returned to growth media for an additional 48 hours. The cells were then fixed with 4% PFA, blocked for non-specific staining with 5% normal goat serum and 1% bovine serum albumin (BSA) in PBS + 0.05% Triton X-100. The cells were then stained with a mouse monoclonal antibody for ZIKV E-protein (clone 1327, Fitzgerald). Virus infected cells were detected using an Alexa-fluor 568 tagged anti-mouse F (ab)$_2$ fragment. Cells were counter stained with DAPI to mark nuclei. Images were collected using an Olympus IX-81 microscope equipped with a Hamamatsu FLASH monochrome CCD

camera and CellSens Dimension software (Ver. 3.1). For all stained samples, individual images were combined into figures using Adobe Photoshop CC.

Behavioral testing

Independent groups of animals began behavioral testing at 60 days post infection (young) or 90–180 days post infection (Adult) or 12–14 months post infection (aged adults). Mice were tested on the rotarod apparatus, followed by open field test (OFT), Novel Object Recognition (NOR), elevated plus maze test (EPM) and finally the social interaction (SI) test, in this order. Each group underwent 1 test per day. For adult and aged groups, there was a six-week delay between NOR and EPM tests due to equipment availability. All mice were tested blindly so the tester did not know the age or prior infection status of the mice.

Rotarod. Locomotor coordination and endurance was assessed using the rotarod test (IITC Life Science; Woodland Hills, CA). Mice underwent 3 consecutive 180 s trials, during which they were placed on a rotating drum (1 ¼ in diameter) that accelerated from 5 rpm to 20 rpm. At least 2 independent reviewers monitored the session and recorded the time the mouse fell off the drum. If the mouse did not fall, a time of 180 s was recorded. The average latency time to fall for the three trials was used for analysis.

Open Field Test (OFT). Horizontal exploratory locomotor activity and anxiety behavior were assessed using the OFT. Mice were placed in the corner of a square arena (40 cm x 40 cm) and allowed to explore freely for 30 min. The trial was recorded with an overhead camera; total distance traveled and time spent in the center of the arena (interior 50%) was automatically scored using TopScan software (CleverSys; Reston, VA) or AnyMaze Software (Stoelting Co., Wood Dale, IL)

Elevated Plus Maze (EPM). Anxiety-like behavior was assessed in the EPM test. The EPM (Stoelting, Inc; Wood Dale, IL) is a raised maze (50 cm above the ground) with two enclosed arms (35 x 5 x 15 cm) perpendicular to two open arms (39.5 x 5 cm) intersected by an open central area (5 x 5 cm). Mice were placed in the center of the maze facing one of the two open arms and recorded with an overhead camera as they freely explored the maze for 10 min. Mice that fell off the maze were immediately returned to the same arm in the same position. Time spent in the open arms and total distance traveled was determined using TopScan software (CleverSys; Reston, VA) or AnyMaze Software (Stoelting Co., Wood Dale, IL)

Novel Object Recognition (NOR). For this test, animals are pre-conditioned one day before the test, by placing the animals in the open field test box, with 2 identical objects (Black spheres or white cubes). The mice freely explore these items for 10 minutes and were then returned to their home cages. To test for novel object recognition, on the next day one of the 2 objects was exchanged for a novel object (eg/ if pre-conditioned with 2 white cubes, then exposed to 1 white cube and 1 black sphere). The animals were then returned to the open field test box for 5 minutes. The trial was recorded with an overhead camera. Time spent with the familiar and novel objects, as well as distance travelled, were automatically scored using TopScan software (CleverSys; Reston, VA) or AnyMaze Software (Stoelting Co., Wood Dale, IL)

Social Interaction (SI). Sociability and social novelty preference were assessed in the SI test as described (Clark et al, 2018). The SI arena (Stoelting, Inc) is a 40 x 40 cm chamber divided into 2 equal sized arenas (18 x 20 cm), connected at their base by a smaller arena (11 x 20 cm) used to traverse between them. Two empty small wire holding cages, weighted at the top, were placed in the far corners of the 2 large arenas. After experimental mice were habituated to the chamber (5 min), previously habituated conspecific, stranger mice were placed in one of the 2 holding cages. Experimental mice then freely explored for 5 min while being recorded with an overhead camera. Total locomotion and time spent near (within 4 cm) the conspecific mouse was determined using TopScan software.

Magnetic Resonance Imaging (MRI). All MRI experimental measurements were performed with an Agilent 7T (300 MHz) horizontal bore small animal MRI (Agilent Inc.; Santa Clara, California) with an open bore of 310 mm and a diameter of 115 mm inside the gradient coil (Resonance Research Inc.; Billerica, MA). The specification of the transmit birdcage RF coil (RAPID MR International Inc.; Columbus, Ohio) is; quadrature driving 12-rung birdcage coil without an RF shield, inner diameter (ID) = 72 mm, inner length = 110 mm, outer length = 120 mm, end-ring width = 5 mm, and rung width = 5 mm. All animals were maintained on 2–3% isoflurane during the tests, while vital signs were being monitored to ensure minimal pain and distress. A spin echo multi-echo multi-slices imaging sequence was used for the in-vivo experiment with TR/TE = 850/10 msec, Number of echo = 5, Number of average = 3, Dummy scan = 0, Data matrix (RO x PE) = 256x256, FOV = 50 x 50 (for Sagittal image) and 40 x 40 (for Transverse image) mm^2, Number of slices = 15, Thickness = 1 mm, Gap = 0 mm, and Scan time = 10 min. 53 sec. The 3D volume mapping and quantitative analysis of fluid volume from acquired MR images were conducted using an open source software, 3D Slicer (ver 4.10)(www.slicer.org; [55]).

Statistical analysis

Statistical analysis for behavioral studies were conducted using both R (R Core Team (2019). R: A language and environment for statistical computing. R Foundation for Statistical Computing, Vienna, Austria. https://www.R-project.org/.) and GraphPad Prism (v. 8.0.1: San Diego, CA). T tests, ANOVA or Mann-Whitney non-parametric tests were used to determine the overall effects of Zika on cytokine levels, behavioral changes and virus titers were used as appropriate. Mann-Whitney non-parametric tests were used to test the effect of Zika within age group. False discovery rate was used to identify gene expression that were significantly modified by the infection. Finally, Spearman's rank correlation coefficient were used to correlate MRI changes, behavior testing and cytokine levels as appropriate. Data are shown as mean +/- SEM; $p < 0.05$ was considered significant. *p<0.05, **p<0.01, ***p<0.001.

Supporting information

S1 Table. Correlations of MRI measurements and Behavior. Spearman's rank correlation were used to compare brain characteristics as measure during MRI volumetric analysis and the indicated behavioral parameters. Statistically significant correlations are indicated with blue, underlined values.
(PDF)

S2 Table. Correlations of inflammatory gene expression and Behavior. Spearman's rank correlations were used to compare immune gene expression and the indicated behavioral parameters. Statistically significant correlations are indicated with blue, underlined values.
(PDF)

S1 Fig. Cellular infiltration and inflammation in the CNS of convalescent ZIKV-infected mice. Sagittal sections from control and ZIKV-infected brains at 12 and 30 dpi. **A.** Sections stained with Iba-1 (red) to mark microglia. Note activation of microglia through the brain at 12 dpi is significantly reduced by 30 dpi in the cerebral cortex, hippocampus and thalamic regions. More focal microglia activation is found in the cerebellum at 30 dpi. **B.** Sections stained with CD45 (green) to mark infiltrating immune cells. Images representative of 3–5 mice.
(TIF)

S2 Fig. Neuropathology in convalescent ZIKV-infected mice. A. Cerebellum of control and ZIKV infected mice stained with DAPI (Blue) and Neurofilament staining (green). Arrow indicates Purkinje cell layer. **B.** Regions in the cerebral cortex and hippocampus stain positively for apoptosis (TUNEL, green) and the activation of microglia (Iba-1+, red) at 22 dpi. These lesions are resolved by 30 dpi. dg = dentate gyrus, hc = hippocampus, OCx = Occipital cortex. Scale bars (A&B) = 500 μm.
(TIF)

S3 Fig. Behavioral data. A. Weight of the animals tested in behavioural studies. **B.** Representative examples of heat tracking maps for 60 dpi mice recorded in the open field and Elevated Plus Maze tests (representative of 6–7 mice/group). The open arm of the maze is labelled. The opposite arm is closed. **C.** Novel Object recognition (NOR). Bars show interaction ratio (Novel:Familiar) as the time spent with new vs familiar objects **D.** Social Interaction Test. Data indicates total movement in the maze and Sociability index (SI, Ratio of Social:Non-social with mice in the maze). Statistical analysis between infected and uninfected groups: T test. * $P < 0.05$.
(TIF)

S4 Fig. Apoptosis and cellular infiltration in sagittal sections of brain. Sagittal sections stained for apoptotic (TUNEL+, green), and immune infiltrating (CD45+, red) cells. Evidence of CD45+ cells and apoptosis in hippocampus and cerebellum convalescent animals at 60 dpi. Image representative of 6 animals.
(TIF)

S5 Fig. Apoptotic foci in cerebellum of ZIKV convalescent mice. A. Confocal image of ZIKV+ foci in cerebellum of 1 ypi ZIKV-infected mice, shows position of TUNEL^{+} cells (apoptosis, green) relative to Iba^{+} microglia (red) and infiltrating CD45^{+} cells (red). Note that microglia proximal to apoptotic lesions shows hypertrophy of the nuclei and short processes consistent with activation (arrow head), while those distant to the lesion show small nuclei and fine processes (arrow). CD45+ infiltrating lymphocytes are also proximal to apoptotic foci. **B.** Individual channels for: Apoptosis (Apop, green), astrocytes (GFAP, red), microglia (Iba-1, red) and infiltrating lymphocytes (CD45+, red) and merged images with orthogonal views, for apoptotic lesions also shown in Fig 5.
(TIF)

S6 Fig. High Sensitivity ZIKV staining indicates specific regions of infection. Images of the cerebellum and brain stain, stained for Iba-1 (green), Zikv, using signal amplification (red) and DAPI (Blue) indicate specific regions of ZIKV infection, associated with foci activated microglia, as indicated in Fig 7.
(TIF)

S7 Fig. ZIKV RNA levels in the cerebral cortex of convalescent mice. Single reaction taqman RT-qPCR for viral RNA performed on total RNA isolated from the cerebral cortex of ZIKV-infected or age-matched control animals. A sub-population of animals demonstrated low levels of viral RNA in the cerebral cortex.
(TIF)

Acknowledgments

Author Contributions

Conceptualization: Derek D. C. Ireland, Mohanraj Manangeeswaran, Daniela Verthelyi.

Data curation: Derek D. C. Ireland, Mohanraj Manangeeswaran, Daniela Verthelyi.

Formal analysis: Derek D. C. Ireland, Daniela Verthelyi.

Funding acquisition: Daniela Verthelyi.

Investigation: Derek D. C. Ireland, Aaron P. Lewkowicz, Kaliroi Engel, Sarah M. Clark, Ha-Na Lee, Ian L. McWilliams, Logan Kelley-Baker.

Methodology: Derek D. C. Ireland, Aaron P. Lewkowicz, Kaliroi Engel, Sarah M. Clark, Adelle Laniyan, Ha-Na Lee, Ian L. McWilliams, Logan Kelley-Baker.

Project administration: Daniela Verthelyi.

Resources: Daniela Verthelyi.

Supervision: Leonardo H. Tonelli, Daniela Verthelyi.

Validation: Leonardo H. Tonelli, Daniela Verthelyi.

Visualization: Derek D. C. Ireland, Aaron P. Lewkowicz, Jacob Sykes.

Writing – original draft: Derek D. C. Ireland.

Writing – review & editing: Derek D. C. Ireland, Mohanraj Manangeeswaran, Aaron P. Lewkowicz, Kaliroi Engel, Sarah M. Clark, Ha-Na Lee, Ian L. McWilliams, Logan Kelley-Baker, Leonardo H. Tonelli, Daniela Verthelyi.

References

1. Hills SL, Fischer M, Petersen LR. Epidemiology of Zika Virus Infection. The Journal of infectious diseases. 2017; 216(suppl_10):S868–S74. https://doi.org/10.1093/infdis/jix434 PMID: 29267914.

2. Sharma V, Sharma M, Dhull D, Sharma Y, Kaushik S, Kaushik S. Zika virus: an emerging challenge to public health worldwide. Can J Microbiol. 2020; 66(2):87–98. Epub 2019/11/04. https://doi.org/10.1139/cjm-2019-0331 PMID: 31682478.

3. Grubaugh ND, Saraf S, Gangavarapu K, Watts A, Tan AL, Oidtman RJ, et al. Travel Surveillance and Genomics Uncover a Hidden Zika Outbreak during the Waning Epidemic. Cell. 2019; 178(5):1057–71. e11. https://doi.org/10.1016/j.cell.2019.07.018 PMID: 31442400.

4. Kama M, Aubry M, Naivalu T, Vanhomwegen J, Mariteragi-Helle T, Teissier A, et al. Sustained Low-Level Transmission of Zika and Chikungunya Viruses after Emergence in the Fiji Islands. Emerg Infect Dis. 2019; 25(8):1535–8. https://doi.org/10.3201/eid2508.180524 PMID: 31310218.

5. (WHO) WHO. Zika epidemiology update 2019. Available from: https://www.who.int/emergencies/diseases/zika/epidemiology-update/en/.

6. Petersen LR, Jamieson DJ, Powers AM, Honein MA. Zika Virus. N Engl J Med. 2016; 374(16):1552–63. https://doi.org/10.1056/NEJMra1602113 PMID: 27028561.

7. Roze B, Najioullah F, Signate A, Apetse K, Brouste Y, Gourgoudou S, et al. Zika virus detection in cerebrospinal fluid from two patients with encephalopathy, Martinique, February 2016. Euro Surveill. 2016; 21(16). https://doi.org/10.2807/1560-7917.ES.2016.21.16.30205 PMID: 27123558.

8. Cao-Lormeau V-M, Blake A, Mons S, Lastère S, Roche C, Vanhomwegen J, et al. Guillain-Barré Syndrome outbreak associated with Zika virus infection in French Polynesia: a case-control study. The Lancet. 2016; 387(10027):1531–9. https://doi.org/10.1016/S0140-6736(16)00562-6 PMID: 26948433

9. Adams Waldorf KM, Nelson BR, Stencel-Baerenwald JE, Studholme C, Kapur RP, Armistead B, et al. Congenital Zika virus infection as a silent pathology with loss of neurogenic output in the fetal brain. Nat Med. 2018; 24(3):368–74. Epub 2018/02/06. https://doi.org/10.1038/nm.4485 PMID: 29400709; PubMed Central PMCID: PMC5839998.

10. Chimelli L, Moura Pone S, Avvad-Portari E, Farias Meira Vasconcelos Z, Araújo Zin A, Prado Cunha D, et al. Persistence of Zika Virus After Birth: Clinical, Virological, Neuroimaging, and Neuropathological Documentation in a 5-Month Infant With Congenital Zika Syndrome. J Neuropathol Exp Neurol. 2018; 77(3):193–8. Epub 2018/01/19. https://doi.org/10.1093/jnen/nlx116 PMID: 29346650.

11. Lebov JF, Brown LM, MacDonald PDM, Robertson K, Bowman NM, Hooper SR, et al. Review: Evidence of Neurological Sequelae in Children With Acquired Zika Virus Infection. Pediatr Neurol. 2018; 85:16–20. Epub 2018/10/23. https://doi.org/10.1016/j.pediatrneurol.2018.03.001 PMID: 30343688.

12. Melo AS, Aguiar RS, Amorim MM, Arruda MB, Melo FO, Ribeiro ST, et al. Congenital Zika Virus Infection: Beyond Neonatal Microcephaly. JAMA Neurol. 2016; 73(12):1407–16. Epub 2016/10/04. https://doi.org/10.1001/jamaneurol.2016.3720 PMID: 27695855.

13. Nielsen-Saines K, Brasil P, Kerin T, Vasconcelos Z, Gabaglia CR, Damasceno L, et al. Delayed childhood neurodevelopment and neurosensory alterations in the second year of life in a prospective cohort of ZIKV-exposed children. Nat Med. 2019; 25(8):1213–7. https://doi.org/10.1038/s41591-019-0496-1 PMID: 31285631

14. Einspieler C, Utsch F, Brasil P, Panvequio Aizawa CY, Peyton C, Hydee Hasue R, et al. Association of Infants Exposed to Prenatal Zika Virus Infection With Their Clinical, Neurologic, and Developmental Status Evaluated via the General Movement Assessment Tool. JAMA Netw Open. 2019; 2(1): e187235–e. https://doi.org/10.1001/jamanetworkopen.2018.7235 PMID: 30657537.

15. Brito CAA, Henriques-Souza A, Soares CRP, Castanha PMS, Machado LC, Pereira MR, et al. Persistent detection of Zika virus RNA from an infant with severe microcephaly—a case report. BMC Infect Dis. 2018; 18(1):388. Epub 2018/08/12. https://doi.org/10.1186/s12879-018-3313-4 PMID: 30097025; PubMed Central PMCID: PMC6086026.

16. Manangeeswaran M, Ireland DDC, Verthelyi D. Zika (PRVABC59) Infection Is Associated with T cell Infiltration and Neurodegeneration in CNS of Immunocompetent Neonatal C57Bl/6 Mice. PLoS Pathog. 2016; 12(11):e1006004. https://doi.org/10.1371/journal.ppat.1006004 PMID: 27855206

17. Clancy B, Finlay BL, Darlington RB, Anand KJ. Extrapolating brain development from experimental species to humans. Neurotoxicology. 2007; 28(5):931–7. Epub 2007/03/21. https://doi.org/10.1016/j.neuro.2007.01.014 PMID: 17368774; PubMed Central PMCID: PMC2077812.

18. Workman AD, Charvet CJ, Clancy B, Darlington RB, Finlay BL. Modeling transformations of neurodevelopmental sequences across mammalian species. J Neurosci. 2013; 33(17):7368–83. Epub 2013/04/26. https://doi.org/10.1523/JNEUROSCI.5746-12.2013 PMID: 23616543; PubMed Central PMCID: PMC3928428.

19. Nem de Oliveira Souza I, Frost PS, Franca JV, Nascimento-Viana JB, Neris RLS, Freitas L, et al. Acute and chronic neurological consequences of early-life Zika virus infection in mice. Sci Transl Med. 2018; 10(444). Epub 2018/06/08. https://doi.org/10.1126/scitranslmed.aar2749 PMID: 29875203.

20. Manangeeswaran M, Kielczewski JL, Sen HN, Xu BC, Ireland DDC, McWilliams IL, et al. ZIKA virus infection causes persistent chorioretinal lesions. Emerging microbes & infections. 2018; 7(1):96. Epub 2018/05/29. https://doi.org/10.1038/s41426-018-0096-z PMID: 29802245; PubMed Central PMCID: PMC5970181.

21. Figueiredo CP, Barros-Aragão FGQ, Neris RLS, Frost PS, Soares C, Souza INO, et al. Zika virus replicates in adult human brain tissue and impairs synapses and memory in mice. Nature communications. 2019; 10(1):3890–. https://doi.org/10.1038/s41467-019-11866-7 PMID: 31488835.

22. Morrison TE, Diamond MS. Animal Models of Zika Virus Infection, Pathogenesis, and Immunity. J Virol. 2017. Epub 2017/02/06. https://doi.org/10.1128/jvi.00009-17 PMID: 28148798.

23. Gorman MJ, Caine EA, Zaitsev K, Begley MC, Weger-Lucarelli J, Uccellini MB, et al. An Immunocompetent Mouse Model of Zika Virus Infection. Cell Host Microbe. 2018; 23(5):672–85 e6. Epub 2018/05/11. https://doi.org/10.1016/j.chom.2018.04.003 PMID: 29746837; PubMed Central PMCID: PMC5953559.

24. Huang H, Li S, Zhang Y, Han X, Jia B, Liu H, et al. CD8(+) T Cell Immune Response in Immunocompetent Mice during Zika Virus Infection. J Virol. 2017; 91(22). Epub 2017/08/25. https://doi.org/10.1128/JVI.00900-17 PMID: 28835502; PubMed Central PMCID: PMC5660488.

25. Carta I, Chen CH, Schott AL, Dorizan S, Khodakah K. Cerebellar modulation of the reward circuitry and social behavior. Science (New York, NY). 2019; 363(6424):eaav0581. https://doi.org/10.1126/science.aav0581 PMID: 30655412.

26. Gill JS, Sillitoe RV. Functional Outcomes of Cerebellar Malformations. Front Cell Neurosci. 2019; 13:441–. https://doi.org/10.3389/fncel.2019.00441 PMID: 31636540.

27. Aragao MFVV Holanda AC, Brainer-Lima AM Petribu NCL, Castillo M, van der Linden V, et al. Nonmicrocephalic Infants with Congenital Zika Syndrome Suspected Only after Neuroimaging Evaluation Compared with Those with Microcephaly at Birth and Postnatally: How Large Is the Zika Virus "Iceberg"? AJNR American journal of neuroradiology. 2017; 38(7):1427–34. Epub 2017/05/18. https://doi.org/10.3174/ajnr.A5216 PMID: 28522665.

28. Johnston MV, Ishida A, Ishida WN, Matsushita HB, Nishimura A, Tsuji M. Plasticity and injury in the developing brain. Brain Dev. 2009; 31(1):1–10. https://doi.org/10.1016/j.braindev.2008.03.014 PMID: 18490122

29. Mavigner M, Raper J, Kovacs-Balint Z, Gumber S, O'Neal JT, Bhaumik SK, et al. Postnatal Zika virus infection is associated with persistent abnormalities in brain structure, function, and behavior in infant macaques. Sci Transl Med. 2018; 10(435):eaao6975. https://doi.org/10.1126/scitranslmed.aao6975 PMID: 29618564.

30. Sánchez-San Martín C, Li T, Bouquet J, Streithorst J, Yu G, Paranjpe A, et al. Differentiation enhances Zika virus infection of neuronal brain cells. Sci Rep. 2018; 8(1):14543. Epub 2018/09/30. https://doi.org/10.1038/s41598-018-32400-7 PMID: 30266962; PubMed Central PMCID: PMC6162312 receives research support from Abbott Laboratories. The other authors disclose no conflicts of interest.

31. Zhao Z, Nelson AR, Betsholtz C, Zlokovic BV. Establishment and Dysfunction of the Blood-Brain Barrier. Cell. 2015; 163(5):1064–78. Epub 2015/11/23. https://doi.org/10.1016/j.cell.2015.10.067 PMID: 26590417; PubMed Central PMCID: PMC4655822.

32. Snyder-Keller A, Kramer LD, Zink S, Bolivar VJ. Mouse Strain and Sex-Dependent Differences in Long-term Behavioral Abnormalities and Neuropathologies after Developmental Zika Infection. The Journal of Neuroscience. 2019; 39(27):5393–403. https://doi.org/10.1523/JNEUROSCI.2666-18.2019 PMID: 31085612

33. Tran LT, Roos A, Fouche J-P, Koen N, Woods RP, Zar HJ, et al. White Matter Microstructural Integrity and Neurobehavioral Outcome of HIV-Exposed Uninfected Neonates. Medicine. 2016; 95(4):e2577. https://doi.org/10.1097/MD.0000000000002577 00005792-201601250-00028. PMID: 26825902

34. Getts DR, Chastain EM, Terry RL, Miller SD. Virus infection, antiviral immunity, and autoimmunity. Immunol Rev. 2013; 255(1):197–209. Epub 2013/08/21. https://doi.org/10.1111/imr.12091 PMID: 23947356; PubMed Central PMCID: PMC3971377.

35. Miller KD, Schnell MJ, Rall GF. Keeping it in check: chronic viral infection and antiviral immunity in the brain. Nature Reviews Neuroscience. 2016; 17(12):766–76. https://doi.org/10.1038/nrn.2016.140 PMID: 27811921

36. Grifoni A, Costa-Ramos P, Pham J, Tian Y, Rosales SL, Seumois G, et al. Cutting Edge: Transcriptional Profiling Reveals Multifunctional and Cytotoxic Antiviral Responses of Zika Virus-Specific CD8(+) T Cells. J Immunol. 2018; 201(12):3487–91. Epub 2018/11/11. https://doi.org/10.4049/jimmunol.1801090 PMID: 30413672; PubMed Central PMCID: PMC6287102.

37. Ireland DDC, Tami C, Pedras-Vasconcelos J, Verthelyi D. CD4 and CD8 T cells mediate distinct lethal meningoencephalitis in mice challenged with Tacaribe arenavirus. Cell Mol Immunol. 2016. https://doi.org/10.1038/cmi.2016.41 PMID: 27569560

38. Wakim LM, Woodward-Davis A, Bevan MJ. Memory T cells persisting within the brain after local infection show functional adaptations to their tissue of residence. Proc Natl Acad Sci U S A. 2010; 107 (42):17872–9. Epub 2010/10/07. https://doi.org/10.1073/pnas.1010201107 PMID: 20923878; PubMed Central PMCID: PMC2964240.

39. Brizić I, Šušak B, Arapović M, Huszthy PC, Hiršl L, Kveštak D, et al. Brain-resident memory CD8(+) T cells induced by congenital CMV infection prevent brain pathology and virus reactivation. Eur J Immunol. 2018; 48(6):950–64. Epub 2018/03/23. https://doi.org/10.1002/eji.201847526 PMID: 29500823.

40. Jurado KA, Yockey LJ, Wong PW, Lee S, Huttner AJ, Iwasaki A. Antiviral CD8 T cells induce Zika-virus-associated paralysis in mice. Nature microbiology. 2018; 3(2):141–7. Epub 2017/11/22. https://doi.org/10.1038/s41564-017-0060-z PMID: 29158604; PubMed Central PMCID: PMC5780207.

41. Wu X, Wu P, Shen Y, Jiang X, Xu F. CD8(+) Resident Memory T Cells and Viral Infection. Front Immunol. 2018; 9:2093–. https://doi.org/10.3389/fimmu.2018.02093 PMID: 30283442.

42. Urban SL, Pewe LL, Harty JT. CD8 T cells are recruited to the central nervous system after peripheral infections and adopt a tissue resident memory phenotype. The Journal of Immunology. 2018; 200(1 Supplement):102.18–.18.

43. Sauder C, Wolfer DP, Lipp H-P, Staeheli P, Hausmann J. Learning deficits in mice with persistent Borna disease virus infection of the CNS associated with elevated chemokine expression. Behav Brain Res. 2001; 120(2):189–201. https://doi.org/10.1016/s0166-4328(00)00370-3 PMID: 11182167

44. Phares TW, Stohlman SA, Hinton DR, Atkinson R, Bergmann CC. Enhanced antiviral T cell function in the absence of B7-H1 is insufficient to prevent persistence but exacerbates axonal bystander damage

during viral encephalomyelitis. J Immunol. 2010; 185(9):5607–18. Epub 2010/09/30. https://doi.org/10.4049/jimmunol.1001984 PMID: 20876353; PubMed Central PMCID: PMC3159959.

45. Maximova OA, Pletnev AG. Flaviviruses and the Central Nervous System: Revisiting Neuropathological Concepts. Annual Review of Virology. 2018; 5(1):255–72. https://doi.org/10.1146/annurev-virology-092917-043439 PMID: 30265628.

46. Pedras-Vasconcelos JA, Puig M, Sauder C, Wolbert C, Ovanesov M, Goucher D, et al. Immunotherapy with CpG Oligonucleotides and Antibodies to TNF- Rescues Neonatal Mice from Lethal Arenavirus-Induced Meningoencephalitis. The Journal of Immunology. 2008; 180(12):8231–40. https://doi.org/10.4049/jimmunol.180.12.8231 PMID: 18523289

47. van den Pol AN, Mao G, Yang Y, Ornaghi S, Davis JN. Zika Virus Targeting in the Developing Brain. J Neurosci. 2017; 37(8):2161–75. https://doi.org/10.1523/JNEUROSCI.3124-16.2017 PMID: 28123079; PubMed Central PMCID: PMC5338758.

48. Phares TW, Stohlman SA, Hinton DR, Bergmann CC. Astrocyte-derived CXCL10 drives accumulation of antibody-secreting cells in the central nervous system during viral encephalomyelitis. J Virol. 2013; 87(6):3382–92. Epub 2013/01/11. https://doi.org/10.1128/JVI.03307-12 PMID: 23302888; PubMed Central PMCID: PMC3592145.

49. Ramakrishna C, Bergmann CC, Atkinson R, Stohlman SA. Control of central nervous system viral persistence by neutralizing antibody. J Virol. 2003; 77(8):4670–8. Epub 2003/03/29. https://doi.org/10.1128/jvi.77.8.4670-4678.2003 PMID: 12663773; PubMed Central PMCID: PMC152147.

50. Pedras-Vasconcelos JA, Goucher D, Puig M, Tonelli LH, Wang V, Ito S, et al. CpG Oligodeoxynucleotides Protect Newborn Mice from a Lethal Challenge with the Neurotropic Tacaribe Arenavirus. The Journal of Immunology. 2006; 176(8):4940–9. https://doi.org/10.4049/jimmunol.176.8.4940 PMID: 16585590

51. Lanciotti RS, Kosoy OL, Laven JJ, Velez JO, Lambert AJ, Johnson AJ, et al. Genetic and serologic properties of Zika virus associated with an epidemic, Yap State, Micronesia, 2007. Emerg Infect Dis. 2008; 14(8):1232–9. https://doi.org/10.3201/eid1408.080287 PMID: 18680646; PubMed Central PMCID: PMC2600394.

52. Zimmerman MG, Quicke KM, O'Neal JT, Arora N, Machiah D, Priyamvada L, et al. Cross-Reactive Dengue Virus Antibodies Augment Zika Virus Infection of Human Placental Macrophages. Cell Host Microbe. 2018; 24(5):731–42 e6. Epub 2018/11/16. https://doi.org/10.1016/j.chom.2018.10.008 PMID: 30439342; PubMed Central PMCID: PMC6394860.

53. Livak KJ, Schmittgen TD. Analysis of Relative Gene Expression Data Using Real-Time Quantitative PCR and the 2-[Delta][Delta]CT Method. Methods. 2001; 25(4):402–8. https://doi.org/10.1006/meth.2001.1262 PMID: 11846609

54. Schindelin J, Arganda-Carreras I, Frise E, Kaynig V, Longair M, Pietzsch T, et al. Fiji: an open-source platform for biological-image analysis. Nat Methods. 2012; 9(7):676–82. Epub 2012/06/30. https://doi.org/10.1038/nmeth.2019 PMID: 22743772; PubMed Central PMCID: PMC3855844.

55. Fedorov A, Beichel R, Kalpathy-Cramer J, Finet J, Fillion-Robin JC, Pujol S, et al. 3D Slicer as an image computing platform for the Quantitative Imaging Network. Magn Reson Imaging. 2012; 30(9):1323–41. Epub 2012/07/10. https://doi.org/10.1016/j.mri.2012.05.001 PMID: 22770690; PubMed Central PMCID: PMC3466397.